RECENT RESULTS ON ZEBRA PATTERN IN SOLAR RADIO BURSTS

G.P.CHERNOV

Key Laboratory of Solar Activity, National Astronomical Observatory, Chinese Academy of Science, 20A, Datun Road, Beijing, 100012, People's Republic of China

(Pushkov Institute of Terrestrial Magnetism, Ionosphere and Radio Wave Propagation, Russian Academy of Sciences (IZMIRAN), Troitsk, Moscow region, 142190, Russia)

gchernov@izmiran.rssi.ru

(Received…. ; Accepted…)

Abstract. This review covers the most recent experimental results and theoretical research on zebra pattern (ZP) in solar radio bursts. The basic attention is given to events with new peculiar elements of zebra patterns received some last years. All new properties are considered in light both known earlier, and new theoretical models. Large-scale ZP consisting of small-scale fiber bursts could be explain by simultaneous including of two mechanism when whistler waves "highlight" the levels of double plasma resonance (DPR). A unique fine structure was observed in the event 13 December 2006: spikes in absorption formed darks ZP stripes against the absorptive type III-like bursts. The spikes in absorption can appear in accordance with well known mechanism of absorptive bursts. The additional injection of fast particles filled the loss-cone (breaking the loss-cone distribution), and the generation of continuum was quenched at these moments. The maximum absorptive effect realizes at the DPR levels. The parameters of millisecond spikes are determined by small dimensions of the particle beams and local scale heights in the radio source. Thus, the DPR model helps to understand several aspects of unusual elements of ZP. But the simultaneous existence of several tens of the DPR levels in the corona is impossible for any realistic profile of the plasma density and magnetic field. Three new theories of ZP are examined. The formation of eigenmodes of transparency and opacity during the propagation of radio waves through regular coronal inhomogeneities is the most natural and promising mechanism. Two other models (nonlinear periodic space – charge waves, and scattering of fast protons on ion-sound harmonics) could be realized in large radio bursts.

Keywords*: solar flare, radio emission, zebra pattern*

1. Introduction

Studies of the fine structure of solar radio bursts are of great importance for both the refinement of the burst generation mechanisms and the diagnostics of the corona plasma. The most intriguing fine structure is undoubtedly the zebra pattern (ZP) in continuous type-IV radio bursts. The nature of the ZP has been a subject of wide discussion for more than 30 years. The ZP in the solar radio emission is the simultaneous excitation of waves at many (up to a few tens) of closely spaced, nearly equidistant frequencies. The basic parameters of ZP in the meter wave band are represented in the atlas of Slottje (1981). The historical development of observations and theoretical models is assembled in the review of Chernov (2006).

The discovery of the superfine structure of ZP, in the form of millisecond spikes was the most significant new effect in the microwave range. The actuality of such a study strongly grew last years in connection with numerous observations of the fast radio bursts (millisecond spikes) during the star flares (Abada-Simon *et al*., 1995). It is amazing that the period of star spikes in the radio burst on the classical red dwarf AD Leo coincides with the period of spikes in the superfine structure of solar zebra stripes (~30 ms) (Osten and Bastian, 2006).

The most comprehensively developed ZP models involve mechanisms based on the double plasma resonance (DPR) and plasma wave – whistlers interaction Chernov (2006). The DPR-based mechanism, which assumes that the upper hybrid frequency in the solar corona becomes a multiple of the electron-cyclotron frequency, has been discussed in most detail. Over the last five year, there appeared a dozen of papers concerning the refinement of this mechanism, because, in its initial formulation, it failed to describe many features of the ZP. Kuznetsov and Tsap (2007) assumed that the velocity distribution function of hot electrons within the loss cone can be described by a power law with an exponent of 8–10. In this case, a fairly deep modulation can be achieved, but the excitation of waves at multiple DPR levels is still impossible. In order to explain the ZP dynamics in the framework of this mechanism, it is necessary that the magnetic field in the radio source varies sufficiently rapidly, which, however, contradicts the fairly low field values determined from the frequency separation between stripes.

In Chernov (1976a; 1990), a unified model was proposed in which the formation of ZPs in the emission and absorption spectra was attributed to the oblique propagation of whistlers, while the formation of stripes with a stable negative frequency drift (the so-called fiber bursts) was explained by the ducted propagation of waves along a magnetic trap. This model explains occasionally observed transformation of the ZP stripes into fibers and vice versa, but fails to describe the existence of ZP stripes whose frequency is stable over a few tens of seconds.

To overcome difficulties arising in different models, a new ZP theory based on the emission of auroral choruses (magnetospheric bursts) via the escape of the Z mode captured by regular plasma density inhomogeneities was recently proposed (LaBelle et al. 2003). This theory, however, fails to explain the high intensity of radiation emitted by separate incoherent sources. In addition, the theory imposes some stringent conditions, such as the presence a large–amplitude ion–acoustic wave.

It is known (Ginzburg and Rukhadze, 1975) that the oscillation spectrum of a nonuniform plasma can be discrete; therefore, the existence of a ZP in the solar radio emission can be attributed to the existence of discrete eigenmodes in the nonuniform solar atmosphere. Several aspects of this mechanism were considered in Laptukhov and Chernov (2006); Barta and Karlicky (2006); Ledenev, Yan, and Fu (2006). In Laptukhov and Chernov (2006), dispersion relations were derived for a discrete spectrum of eigenmodes of a spatially periodic medium in the form of nonlinear structures formed due to the onset of thermal instability. The spectrum of eigenfrequencies of a system of spatially periodic cavities is calculated, and it is shown that such a system is capable of generating a few tens of ZP stripes, the number of which is independent of the ratio of the plasma frequency to the gyrofrequency in the source.

In the present paper, an attempt is made to evaluate which model most adequately describes the observational data and find out where the ZP stripes form

(during the excitation of waves in the source or in the course of their further propagation). Calculations show that the DPR-based mechanism fails to describe the generation of a large number of ZP stripes in any coronal plasma model. Here, it is shown that the new varieties of ZP succeeds in explaining within the framework of known mechanisms taking into account the special features of plasma parameters and fast particles in the source. From other side, the formation of ZP stripes due to the radio wave propagation through the coronal heterogeneities can be recognized as the most natural mechanism of ZP. The mechanism related to the excitation of discrete eigenmodes of a periodically nonuniform plasma (Laptukhov and Chernov, 2006) can yield the observed number of harmonics. However, in this case, only the possibility of generating harmonics in a one-dimensional stationary problem is considered, i.e., the frequency dynamics of stripes is not analyzed.

For last three years some new varieties of ZP have been registered. Now it is necessary to estimate possibility of their interpretation taking into account all known models of ZP.

2. New observations

2.1. 24 July 2004 Event

Chernov et al. (2008) analyzed strange fiber structures in four events in decimeter range when small-scale fibers are organized into large-scale ZPs. They used spectral observations of the new Chinese spectrometer (Huairou station of NAOC, Beijing) in the range of 1.1 – 2.0 GHz with extremely high resolution of 5 MHz and 1.25 ms (Fu *et al*., 2004).

Figures 1 demonstrate a new variety of stripes in emission in the event on 24 July 2004. At the beginning of the event, separate narrow-band stripes (small fibers) were located along the frequencies, forming almost instantaneous pulsations (around 06:04:20 UT); then they were decomposed and aligned along the inclined straight lines that are parallel to the individual small fibers. At the end of this time interval the small fibers formed almost braided ZP (around 06:04:26 UT). The circular polarization of the fibers was dominantly of right-hand sign.

One second later (Figure 1a), they were located once more along the inclined straight lines (06:04:27.0 – 06:04:28.5 UT), and a new special feature was seen two seconds later (06:04:30 UT): they were localized along the straight lines, but with the reverse (positive) drift. In one more second (06:04:31 – 06:04:33 UT), this special feature was already clearly the basic prevailing structure (Figure 1b) which is almost regarded as large-scale ZP stripes drifting to higher frequencies with the speed of about 270 MHz s^{-1}. These structures were terminated at a certain high-frequency boundary which drifted to lower frequencies approximately with the speed of – 67 MHz s^{-1}.

In Figure 1 only right polarization channels are presented because the polarization degree was 100%. The fiber structure appeared as a forerunner of the rise of continuum which continued for more than three minutes, but no more fine was observed.

The flare of M1.0 1F class has occurred at 06:01 – 06:04 – 06:10 UT in the active region (AR) 10652 (N07W20). The analyzed fibers structure was observed after several strong pulsations at the very beginning of the smooth rise of a flare continuum in the unpolarized emission whose duration was about 5 minutes.

According to the spectral data of IZMIRAN in the frequency range of 270 – 25 MHz, the pulsations had a continuation in the meter-wave range in the form of type III bursts, where they stopped at frequencies near 200 MHz in the form of J-bursts. Later the flare continuum lost any fine structure, and the event ended, without type II burst and any coronal mass ejection (CME).

In the absence of spatially-resolved radio observations, the position of the radio source can be inferred from Figure 2, where the image of the flare in the chromosphere of the Transition Region and Coronal Explorer (TRACE 1700 Å data) (Strong *et al*. 1994) at the moment 04:07 is superimposed on the magnetogram (Solar Flare Telescope, NAOJ/Mitaka). Three bright flare kernels (dark blue patches) are located to the west of the preceding sunspot of this AR, above the quadrupole-like structure of the magnetic field with a peculiar X- point at the center of the flare region.

The two flare kernels were located above the S- magnetic polarity; therefore the radio emission of right circular polarization should correspond to the ordinary wave mode. The flare kernels in the 195Å images were also located exactly above the bright regions seen in the 1700 Å images, and the radio source in right circular polarization at 17 GHz (Nobeyama Radio Heliograph) was also located in this place. The largest radio flux was recorded in decimeter and meter ranges, indicating the magnetic reconnection high in the corona. As a matter of fact, in the 1700 Å images we see bright tops of the flare loops. The decimeter radio source is expected to be found below the flare current sheet (where the acceleration of fast particles would take place) and in the lower closed magnetic loops, of which we see the bright tops in Figure 2. The positive frequency drift of the large scale ZP stripes may be caused by the downward motion of a plasma ejection from the reconnection region with the Alfvén velocity. This ejection would meet on its way a flare loop arcade that was expected to be rising. The high-frequency boundary of the termination of emission can be the consequence of this collision.

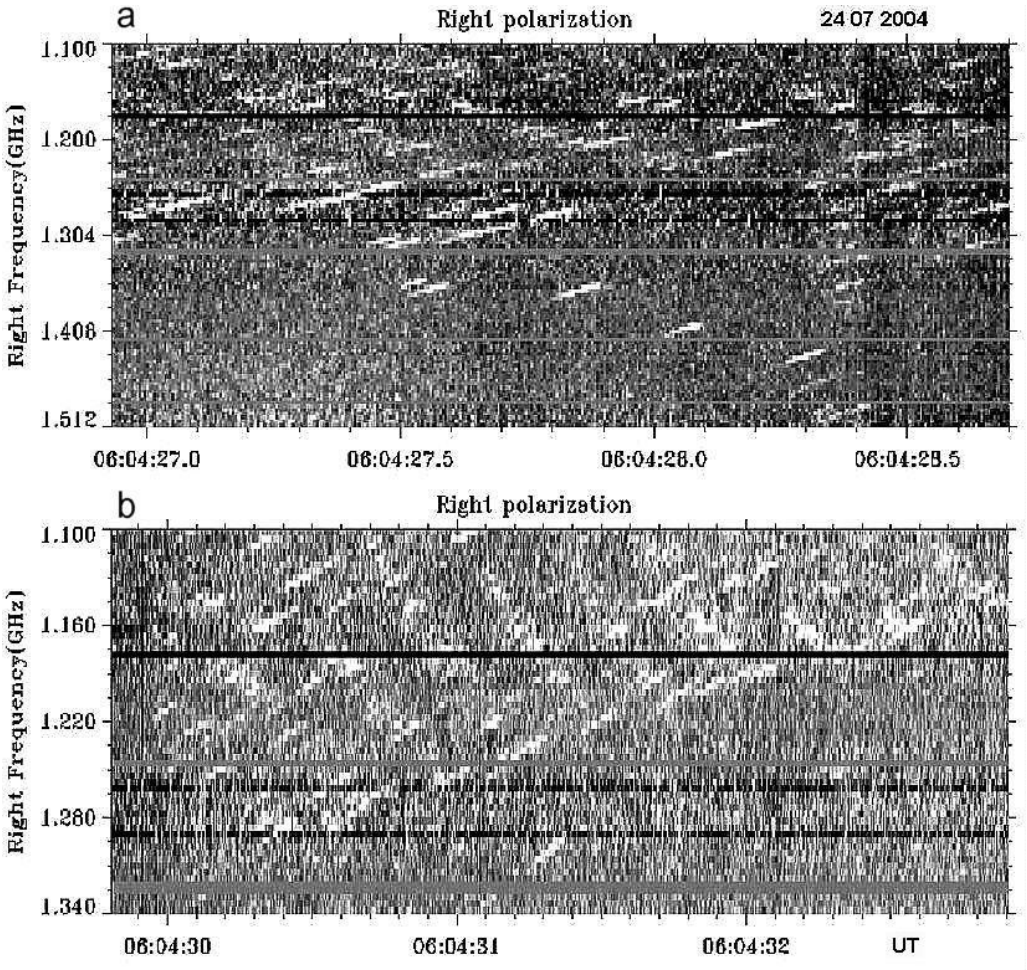

Figure 1 (*a*) Dynamic spectrum in the range 1.100 – 1.512 GHz in left and right circular polarizations recorded by the spectrometer of NAOC on 24 July 2004. (*b*) The continuation of the 24 July 2004 event in the range 1.100 – 1.340 GHz in the right- circular polarization (the radio emission is fully polarized).

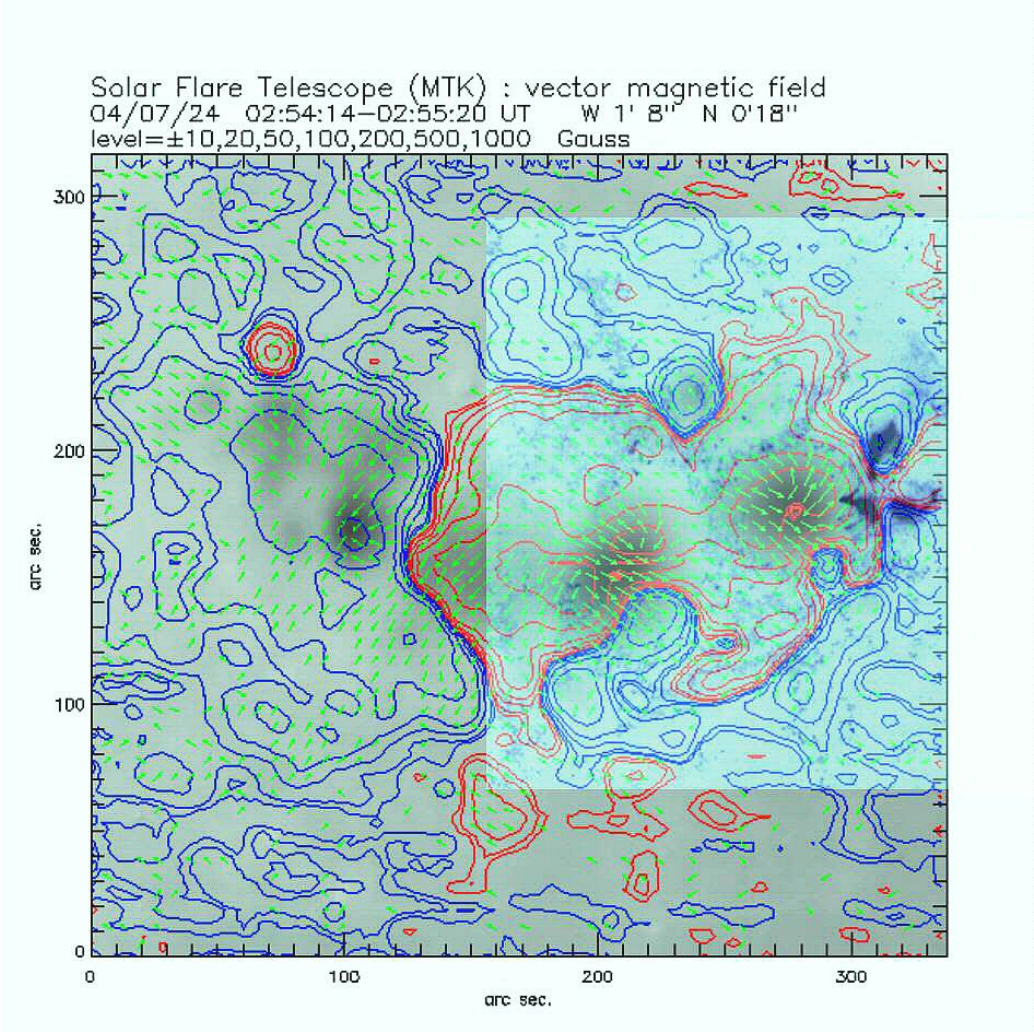

Figure 2 A TRACE 1700 Å image of the flare on 24 July 2004 in the chromosphere at the moment 04:07 UT, superimposed on the magnetogram (Solar Flare Telescope, NAOJ/Mitaka).

2.2. 3 November 2004 Event

This event was most powerful and most prolonged, with diverse fine structures with the duration of about 2 hours, in the course of repetitive brightenings of the flare. We selected for the analysis only its first part (with the duration about 25 minutes), at the beginning of which small-scale fibers were observed (Figure 3), and as in the previous events also as a forerunner of the entire event.

The first glance at Figure 3 reveals certain similarity to the event of 24 July 2004: at first the small-scale fibers occurred chaotically scattered along the frequencies, then they localized at some frequencies and formed a large-scale ZP stripes, and at the end they broke up again to separate chaotic fibers, which gradually (during ≈ 1.5 minutes) broke up to a cloud of chaotic spikes. The essential difference lies only in different polarization. Here, it was of moderate right-hand sign.

Figure 4 helps to better estimate the parameters of the small fibers that composed the large-scale ZP. The time profiles at the fixed frequency of 1.216

GHz show that all profiles are symmetrical, and have an almost Gaussian shape. The frequency drift of fibers was stable and constant, ≈ – 270 MHz s^{-1}, and for large-scale ZP it was ≈ 630 MHz s^{-1}.

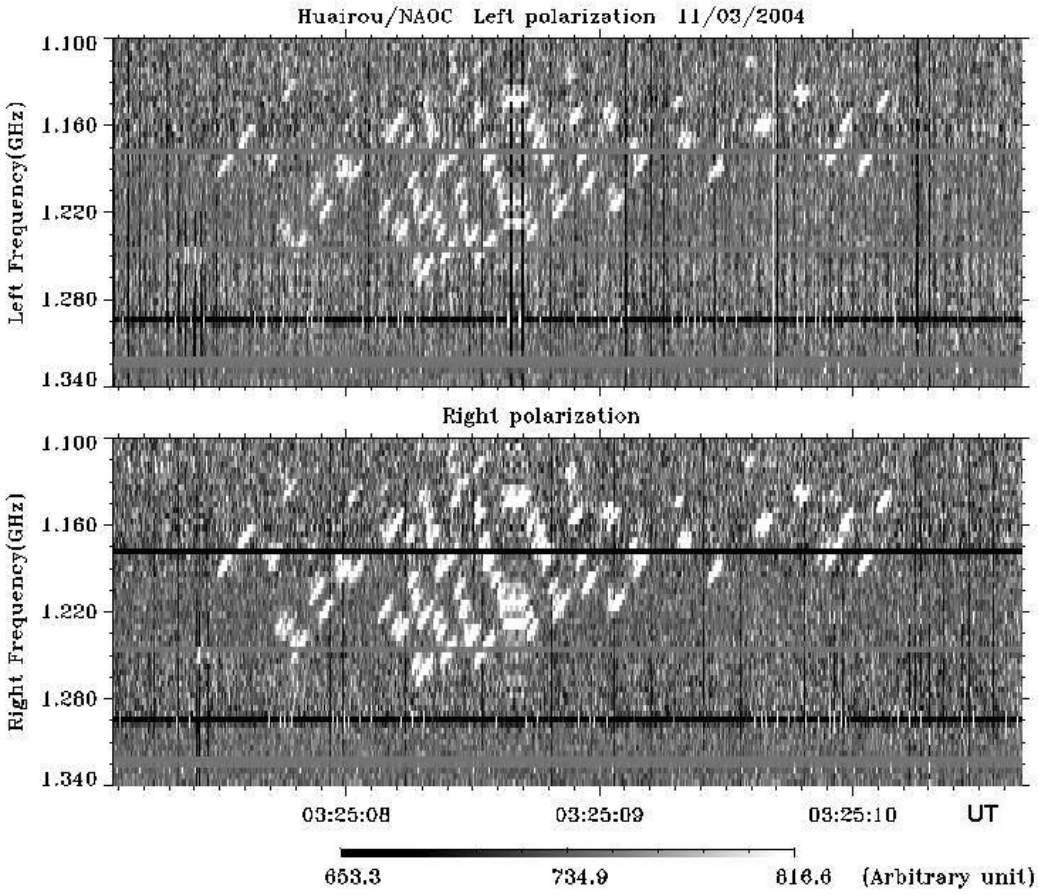

Figure 3 The beginning of the 3 November 2004 event in the frequency range 1.100 – 1.340 GHz, showing moderate right-hand polarization: the small-scale fibers are re-grouped into large-scale ZP stripes.

The flare of M1.6 1N class has occurred at 03:23 – 03:35 – 03:57 UT in AR 10696 (N09E45). The analyzed fiber structure was observed at 03:25:07 UT at the very beginning of the smooth rise of a flare continuum in the non-polarized emission whose duration was about 25 minutes. According to Culgoora spectral data, strong type II bursts began at 03:33 UT at frequencies near 120 MHz (estimated shock speed 750 km s^{-1}), accompanied by a powerful CME (SOHO/LASCO C2) after 03:54 UT (whose estimated speed was 918 km s^{-1}).

After about 03:30 UT the polarization of the fine structure changed sign, and the left-handed polarization became predominant. The dynamics of flare processes can be tracked according to Figures 5a and 5b, in which for two moments at the beginning of the event, the sources of hard X-rays (RHESSI/HXR) in the 6.0 – 7.0 keV energy band are superimposed on the 17 GHz (Nobeyama) radio map. Figure 5a shows that at 03:26 UT the radio source had a triple structure (in accordance with the distribution of sunspots in the AR) with a big source of predominantly right-hand circular polarization above the following spot of the S-polarity. A single HXR- source (A) was located above this radio source. At 03:30 UT

(Figure 5b) a new HXR source (B) appeared in the south-western portion of the AR. Thus, the strengthening of the radio source at this moment was connected with the development of the flare above the small leading spot of N-polarity. In the higher energy band 14.0 – 16.0 keV even two new sources have appeared in the same location. So, it is possible to conclude that the radio emission corresponded to the ordinary wave mode both at the beginning and in the maximum of the event.

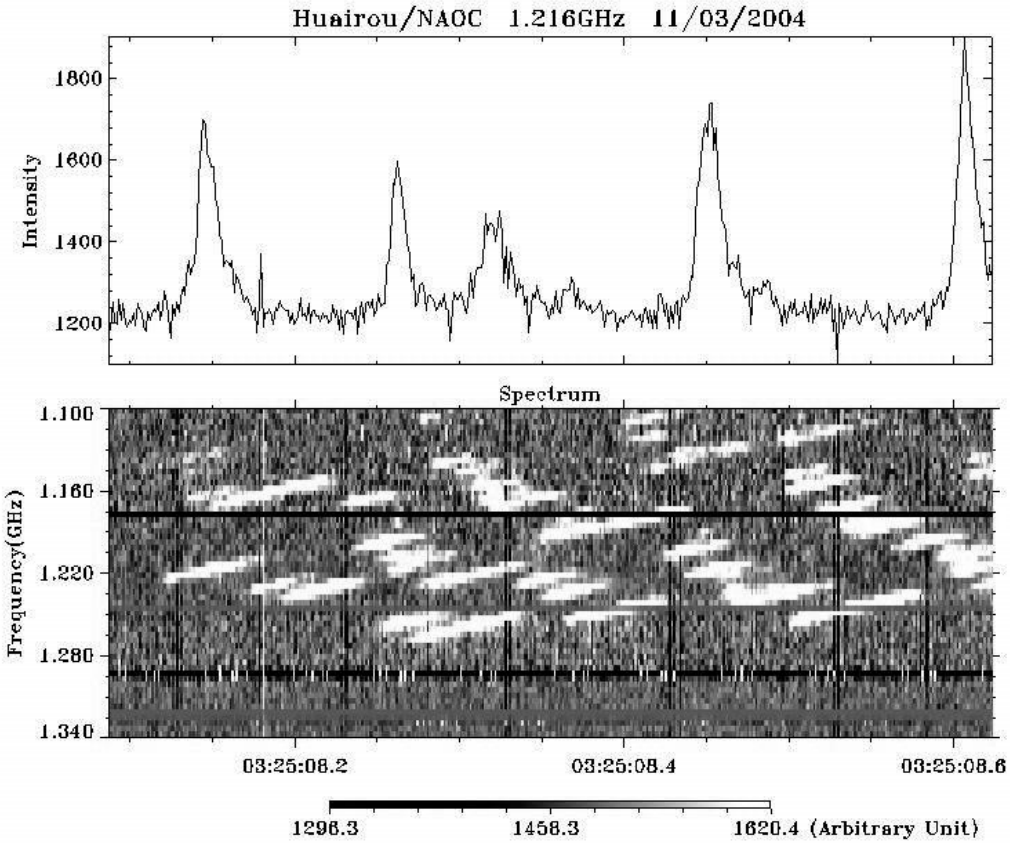

Figure 4 The magnified dynamic spectrum (bottom) and the time profile at 1.216 GHz (top) of the fiber structure on 3 November 2004.

We can derive the following conclusions from the observations of two events with small-scale fiber bursts as a substructure of large-scale ZP:

- Narrowband fibers drift almost always to lower frequencies with the speed that is typical in usual fiber bursts, and sometimes they are similar to the ropes of fibers in the meter range.
- In two events the fibers evolved from a chaotic features in the dynamic spectrum to a regulated structure (in the form of large-scale ZP stripes) and again to the disorder, being gradually converted into the spike-bursts.

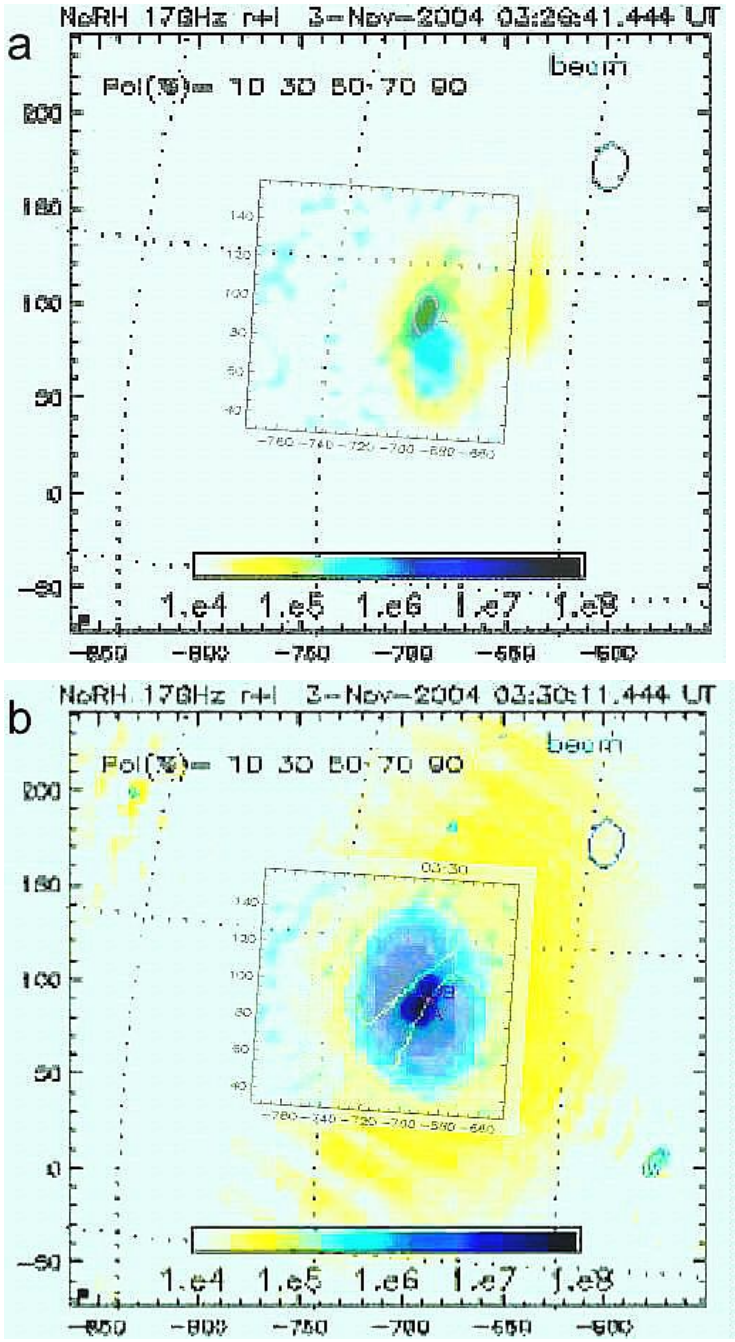

Figure 5 17 GHz radio maps (Nobeyama) at two moments at the beginning of the 3 November 2004 event. The sources of hard X-rays (RHESSI HRS) in the 6.0 – 7.0 keV energy band are superimposed (green patch in (*a*) and dark blue patch in (*b*)).

- Large-scale ZP was limited at high frequencies by a boundary drifting to lower frequencies with the speed of – 70 to – 90 MHz s^{-1}.
- The radio emission are moderately or strongly polarized.
- The fiber structure appeared as a forerunner of the entire event.
- The fibers, as well as large-scale ZP, do not reveal absorptions at the low frequency edge.
- A superfine structure in small-scale fibers was not detected with a time resolution of 1.25 ms.

In two other events (22 December 2004 and 31 October 2004) small-scale fibers can be regarded as a fine structure in type III bursts and broadband pulsations.

2.3. 13 December 2006 Event

2.3.1. Introduction

The most recent large flare of the 23rd cycle was observed on December 13, 2006 (02:10 – 05:10 UT) in the active region NOAA 10930 (S05W24–27). This was an unusual event by its importance (X3.4/4B) and fast coronal mass ejection (CME). The flare provided also the richest material for the analysis of fine structures of radio emission in the microwave range. Numerous spikes in absorption of millisecond duration are the main feature of radio emission observed during the decay phase of the flare. The Solar Broadband Radiospectrometer (SBRS) in the range of 2.6–3.8 and 5.2–7.6 GHz (Huairou station, NAOC) carried out the radio observations (Fu *et al*. 2004). The frequency resolution of the SBRS is 10 MHz, and the cadence is 8.0 ms.

During this long-lasting event different types of common fine structures were observed (e.g. spikes in emission, usual zebra-pattern and fast pulsations). However, on the decay phase together with the spikes in emission, spikes in absorption began to appear. The latter were first randomly distributed in the frequency range 2.6–3.8 GHz, then they exhibited fast pulsations and trajectories of type III-like bursts in the dynamic spectrum. Furthermore, numerous type III bursts in absorption were observed for about one hour.

The impulsive phase of this event with some fragments of zebra patterns has already been described by Yan, *et al.*(2007). Fast radio pulsations were examined in Tan *et al.* (2007). They assumed that a resistive tearing-mode oscillation in the current-carrying flare loops modulated the microwave emissions and formed the pulsating structures. The positions of X-points is between two magnetic islands. There are many X-points in each flare loop.

The spikes in emission and fiber bursts were studied by Wang *et al.* (2008). Chen and Yan (2008) already reported the absorptive spikes in this event. The type III-like burst in absorption had been explained by Chen and Yan (2008) as a fragmentary injection of new particles in a loss-cone leading to quenching of the loss-cone instability of plasma waves at the upper-hybrid frequency. Parameters of the bursts in absorption (instantaneous frequency bandwidth and duration, frequency drift *etc*.) depend on parameters of new beams of particles.

A general description of absorptive spikes in this event was carried out by Chernov *et al*. (2009). It should be understood the reason for the appearance of spikes in absorption at the decay phase of the event. It was necessary to estimate how the physical parameters vary in the event, and how the type III-like bursts are formed from the absorptive spikes (with elements of ZP stripes).

The first spikes in absorption appeared at 02:53:08 UT. Further, over more than one hour, different combinations of the spikes in absorption and the type III-like bursts in absorption and in emission were observed. The latter appeared simultaneously and both with positive and negative frequency drift. For the analysis, it is important to know what kind of specific features of the flare were associated with the appearance of bursts in absorption.

Figure 6 shows the timing and frequency range of fine structures in the dynamic spectrum of the whole event. It is evident that spikes in emission (yellow bars) were observed over the whole event while the spikes in absorption (red) were only in the decay phase. Typical fragments of bursts in absorption are shown in Figures 8 and 9. It should be noted that the usual fine structures in emission, zebra pattern (green bars in Figure 6) and fiber bursts (blue bars) were observed over the whole event as well (see also Figures 10 and 11).

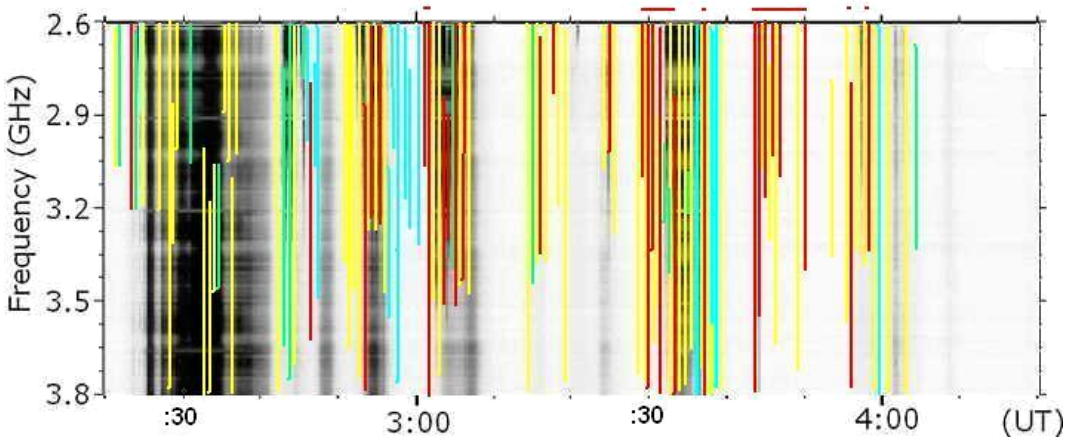

Figure 6 The dynamic spectrum of the whole event 13 December 2006 in the frequency range of 2.6 – 3.8 GHz. The emission is displayed in a negative picture (darker means stronger emission). The color bars indicate timing and frequency range of fine structures: yellow – spikes in emission, red – spikes in absorption, blue – fiber bursts, green – zebra pattern. The red horizontal bars at the top show the time intervals when spikes in absorption formed type III-like bursts (from Chernov *et al*., 2009).

2.3.2. New flare brightening in TRACE- images

The further dynamics of the flare was outlined in more detail with the TRACE-images in the 195 Å passband. They show flare loops with temperature of $1.8 \cdot 10^6$ K. Six images taken from TRACE catalog data (http://trace.lmsal.com/trace_cat.html) are shown in Figure 7.

According to the TRACE images of the 195 Å passband at the impulsive phase, the flare consisted of many bright kernels distributed over the entire active region and bright large-scale loops, that extended predominantly from the north-west to the south-east, connecting to distant spots. During the impulsive phase in the eastern part of the active region, five consecutive flare brightenings were observed. After approximately 02:40 UT the TRACE images show thin loops (arcades) along the large-scale X-ray loop which began to be formed westwards. After approximately 02:47 UT, the new loops started to appear successively towards west.

On the first TRACE 195 Å image in Figure 7 (02:48 UT) new bent loops appeared in the western part of the region and began to ascend. The three images (03:02, 03:20, and 03:23 UT) illustrate the subsequent rising of these bent loops and some changes above them which suggest rapid flows. At 03:20 UT the bent loop did look like a cusp for the first time.

After approximately 03:36 UT, the restoration of the magnetic structure began, and the bent loops (with a possible apex) began to descend. At 04:23 UT, the bent loops descended finally, and the burst activity completely ceased after that. During this time, about ten peaks of radio emission occurred at 2.84 MHz

(Figure 1 in Yan, *et al*. (2007)). Diverse bursts in absorption were observed practically during each peak.

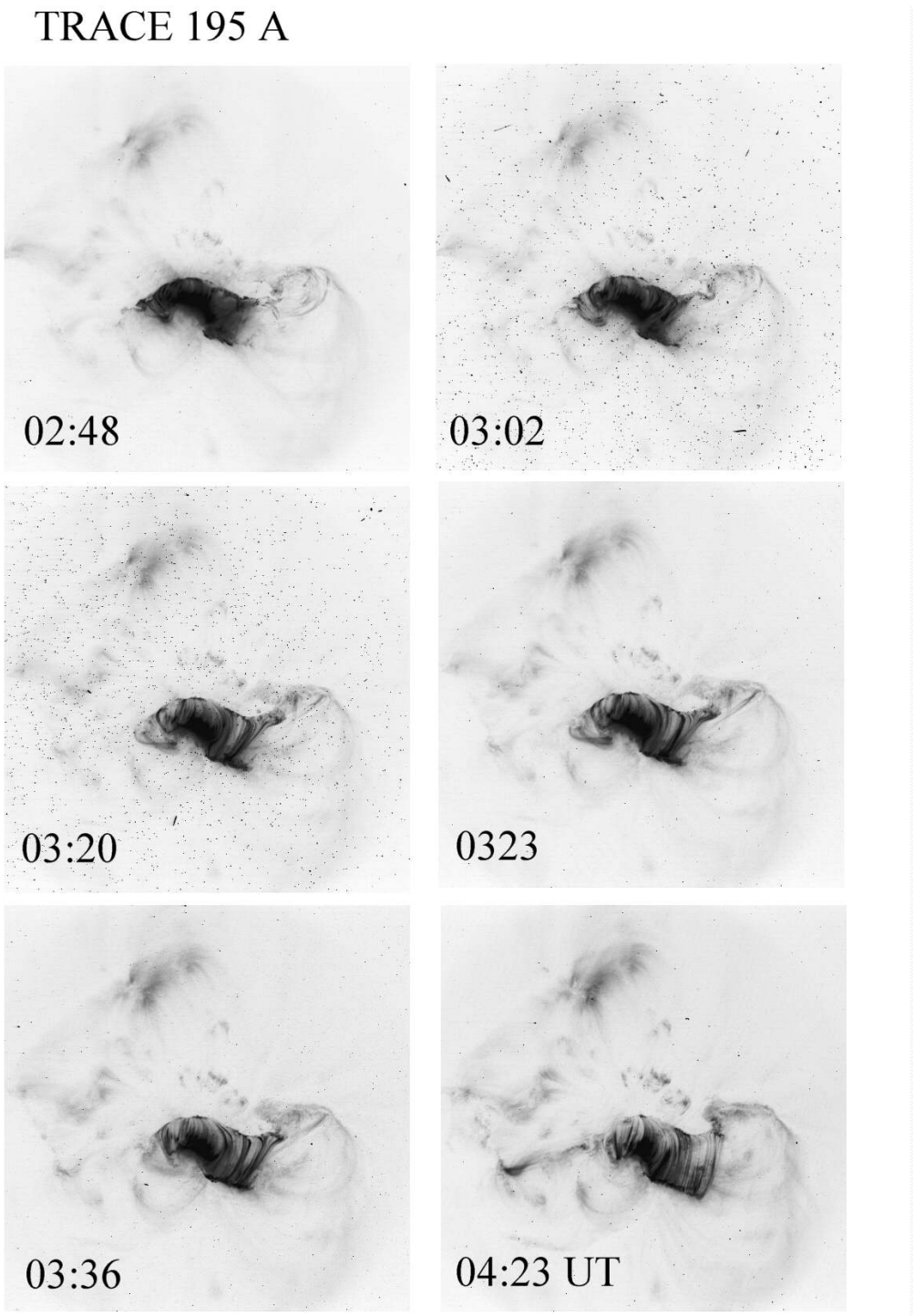

Figure 7 The development of the flare in the western part of the post-flare arcade in the TRACE EUV passband 195 Å (from Chernov *et al*., 2009).

According to the Nobeyama Radio Heliograph (NRH) data at 17 GHz (see Figure 2 in Chen and Yan (2008) the peak of the radio continuum burst was located above northern flare ribbon in the negative magnetic polarity. During the new flare brightening at 03:28 UT the radio source revealed asymmetry with a second maximum above the western part of the northern flare ribbon. This

location coincides with the new helmet-shaped loop in the western part of the loop arcade after 03:23 UT (Figure 7).

2.3.3. Features of bursts in absorption

Figures 8 and 9 show the appearance and the development in detail in time of spikes in absorption according to the data of SBRS (in the frequency range 2.8–3.6 GHz). Only the right-handed circular polarization (RHCP) components of SBRS are shown because during the decay phase of the event the emission was fully right-handed polarized.

The first spikes in absorption appeared at 02:53:08 UT (Figure 8a). All spikes had different frequency bandwidth, from a point-like (in one pixel with the sizes of 10 MHz, 8 ms) to 400 MHz, but no bursts showed frequency drift. Therefore, each spike represents an instantaneous frequency bandwidth. Most of them were scattered randomly in the frequency and time domains. During the time interval shown in Figure 8a, we did not notice specific patterns in appearance of spikes in absorption and in emission. At the beginning and the end of the interval, we observed predominantly spikes in absorption. In the middle of the considered time interval, the spikes in absorption and emission appear simultaneously at different frequencies and they distributed randomly with respect to each other.

After 03:01:28 UT, the non-drifting spikes began to be built along the inclined trajectories and to form the absorptive bursts, similar to type III bursts, shown in Figure 8b. The analysis of such bursts in the interval 03:01:28 – 03:01:37 UT is very important. The first group of isolated spikes at 03:01:29.5 UT were built along two type III-like trajectories, with different frequency separation between spikes. Then, the large dark type III-like burst in absorption with longer duration of 0.12 s appeared. The subsequent two trajectories consisted of isolated spikes again. In addition, several following type III trajectories were accompanied by spikes with diversified frequency bandwidths and frequency drift rates (see the continuation of possibly similar activity in Figure 8e).

It is important to note that the isolated spikes along the type III trajectories were shifted in frequency with separations approximately equal to the bandwidth of the spikes (≈ 80 MHz). However, in the following type III-like large bursts, they overlapped in frequency (they became more broad-banded, ≈ 160 MHz). The strongest spikes appeared one after another, *i.e*., with the period equal to their duration (8 ms). Thus, it is not completely excluded that spikes in actuality have smaller bandwidths and shorter duration, due to the limited frequency and time resolution of the instrument (10 MHz and 8 ms). After 03:01:31 UT, clouds of spikes in emission began to appear, with approximately the same parameters, but they did not form type III bursts in emission.

In the interval 03:03:00 – 03:03:10 UT, fragments of the large-scale ZP in emission appeared in the HF edge of the powerful emission (the top panel in Figure 10). Large-scale ZP means that the frequency separation between stripes is around 170 MHz, the largest value found in this event (see Table 1 in Yan *et al.* 2007). Numerous spikes in emission and absorption were seen superimposed on ZP stripes. The spikes in absorption constituted the absorption stripes of the ZP. Previously, only spikes in emission were reported as substructures of ZP emission stripes (Chernov *et al*., 2003; Chernov *et al.*, 2005).

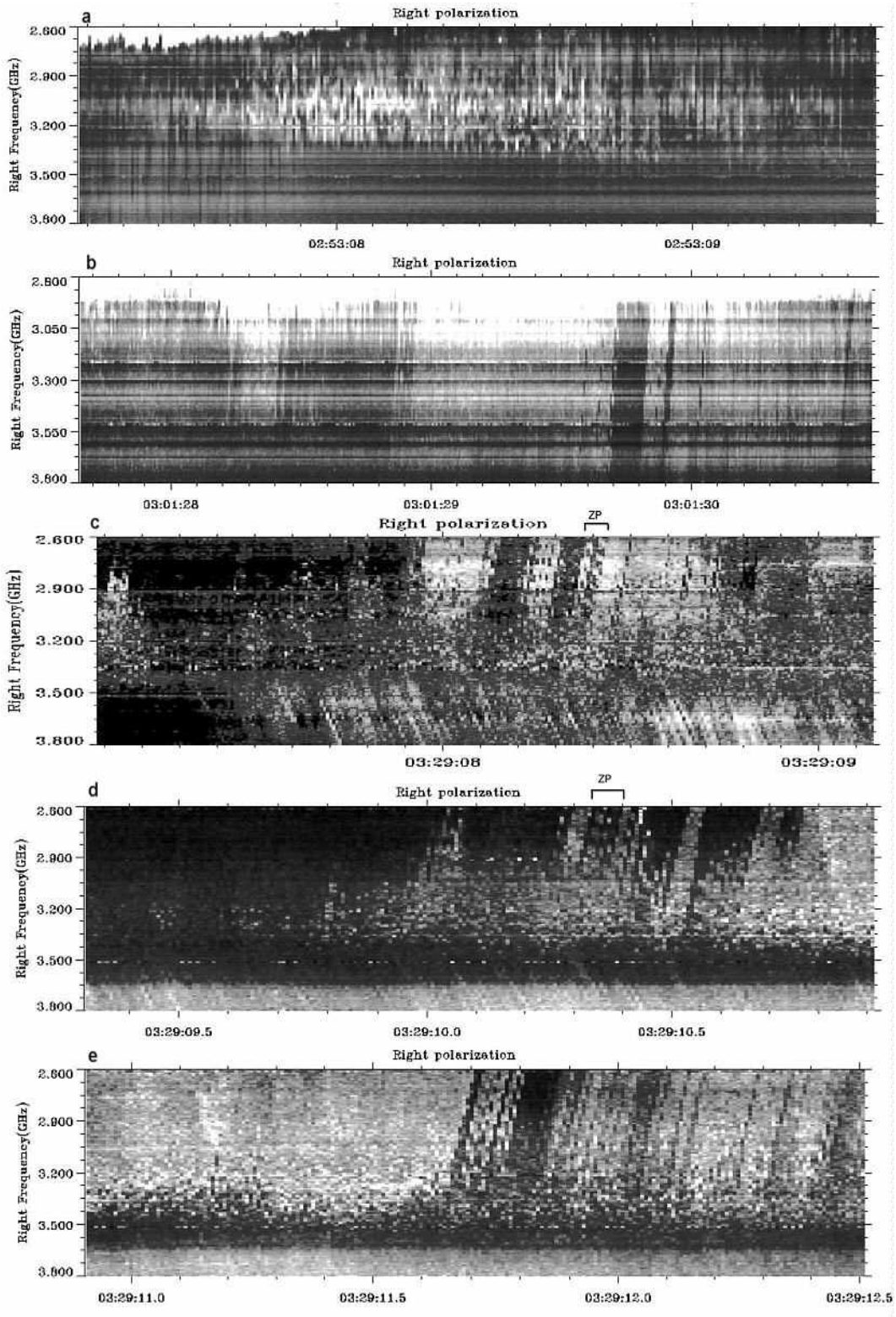

Figure 8 Dynamic spectra of the component of right-handed circular polarization in 2.6 – 3.8 GHz showing the consecutive development of the absorptive spikes at 02:53 UT and of type III-like busts consisting of spikes in absorption at 03:01 and 03:29 UT. The frequency and time scales are different in different panels (from Chernov *et al*., 2009).

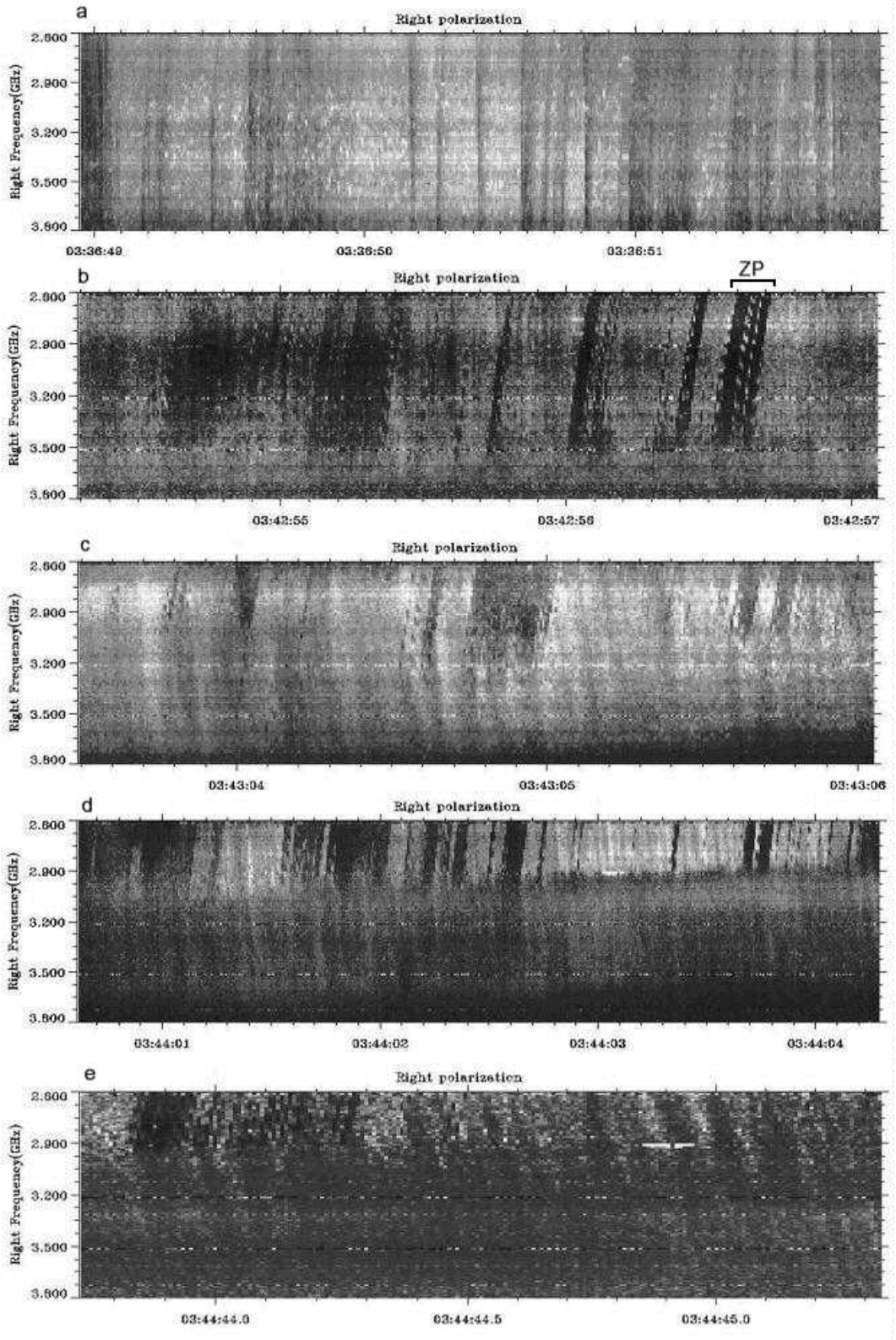

Figure 9 The continuation of the development of the right-hand circularly polarized component in 2.6 – 3.8 GHz in the time interval 03:36 – 03:44 UT showing the absorptive type III-like bursts accompanied by the reverse-drifting bursts in emission and absorption (from Chernov *et al*., 2009).

Such a complex combination of different structures continued up to 03:24:30 UT, when the reverse drifting bursts in absorption appeared as prevailing

structure. However, in contrast to type III-like bursts in absorption, they did not show clear spike substructures. To be more precisely, maybe the spikes were not resolved by the instrument, or perhaps substructures do not exist at all. In the next few seconds the reverse-drifting bursts in emission appeared, and alternated with the bursts in absorption almost over the entire frequency range of the spectrometer. Until 03:25:22 UT, the range of the intermittent reverse-drifting bursts was from 2600 to 3000 MHz.

After 03:29 UT a new powerful flare brightening began, and in the mean time bursts in absorption with new properties appeared (Figures 8c and 8d). The frequency of ≈3400 MHz became the "boundary" between the burst of the opposite drifts. The bursts in absorption with the fast direct (negative) drift appeared at the higher frequencies, and the reverse-drifting bursts in emission and absorption appeared at the lower frequencies. We did not notice any correlation between bursts of different drift. Moreover, the drift to higher frequencies of the latter bursts was approximately three times slower, of 3.6 GHz s^{-1}, and they actually looked like classical fiber bursts with typical absorption from their LF edge (Chernov, 2006) but with reverse drift. The low-frequency bursts in absorption were composed of spikes with almost no frequency separation (03:29:08.15 – 03:29:08.25 UT). The spikes that formed the type III-like bursts had a wide range of parameters and showed no regularity in appearance. The spikes, as the substructures of type III-like bursts, are clearly visible in Figures 12 and 13 with enlarged spectra and time profiles at two fixed frequencies.

However, at 03:29:08.4 – 03:29:08.5 UT in Figure 8c in the type III-like bursts (in the frequency range 2.60 – 3.05 GHz) it is possible to distinguish absorptive ZP-like stripes (noted on top by symbols ⌐¬ and ZP), which drifted to higher frequencies and consisted of spikes. A similar but short fragment of ZP-like stripes repeated at 03:29:10.3 in the frequency range of 2.60 – 2.90 GHz (Figure 8d).

In the subsequent two minutes (03:30 – 03:32 UT) the powerful pulsations in emission (partially interrupting with the broadband pulsations in absorption) and clouds of narrow-band spikes in emission were observed. At 03:32:16 UT, several stripes of usual ZP appeared (the second panel in Figure 10) with the narrow frequency separation (of ≈40 MHz). Numerous spikes in emission and absorption accompanied these several ZP stripes.

In Figure 9, further development of bursts in absorption is represented, when the helmet-shaped flare loop on the western edge of the arcade began to descend (the image at 03:36 UT in Figure 7). In Figure 9a, pulsations in absorption (or type III-like bursts), are seen against the background of a large cloud of spikes in emission. The pulsations did not reveal a strict periodicity, but the spikes in absorption are visible as the substructures of pulsations.

Against the background of such pulsations during 03:36:57 – 03:36:58 and 03:37:04 – 03:37:05.5 UT, the type III-like trajectories containing isolated almost point-like spikes in emission appeared. Again, the classical fiber bursts at 03:37:12 – 03:37:25 UT against the background of pulsations in emission and absorption were observed (a part of these fibers is shown in the middle panel of Figure 11), when the flare brightening was decaying. These fiber bursts were gradually transformed into broadband stripes predominantly in absorption with the decreasing frequency drift. Then the reverse-drifting (almost through entire range) fiber bursts appeared again during 03:37:34 – 03:37:38 UT. Further, the fibers against the background of powerful pulsations and the clouds of spikes in emission (03:37:49 – 03:38:10 UT) appeared again.

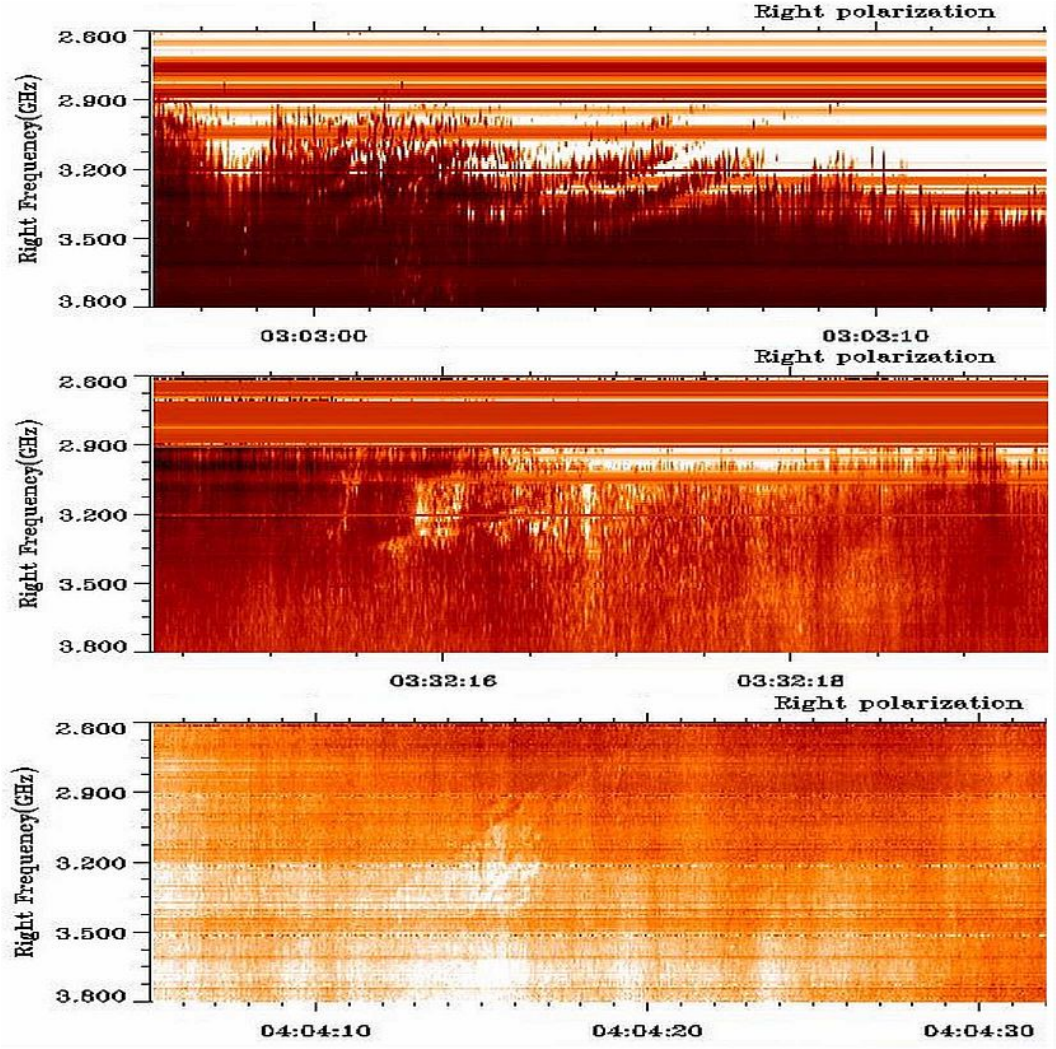

Figure 10 Enlarged spectra showing the ZP at the post-maximum phase of the event. The top panel shows spikes in emission and absorption superimposed on ZP stripes. The spikes in absorption constituted the absorption stripes of the ZP. Numerous spikes in emission and absorption were accompanied several ZP stripes in the middle panel. Note the unusual (braded) ZP in emission and absorption - in the bottom panel (from Chernov *et al*., 2009).

This entire dynamics is very important for understanding the appearance and development of the uncommon bursts in absorption. During three more minutes, the clouds of strong spikes in emission were observed. In the end of this interval, broadband pulsations in emission and absorption with the reverse drift accompanied these clouds. The pulsations were followed by the type III-like bursts in absorption which consisted of non-drifting spikes in absorption. During the time interval 03:42:56.5 – 03:42:56.7 UT (Figure 9b), spikes in absorption formed the absorptive ZP-like stripes. In this time interval, all features of the type III-like bursts in absorption noted above (during the different moments) were seen.

The initial HF boundary of the absorptive bursts was slightly displaced downwards, up to ≈3500 MHz. In the middle part of this spectrum, weak non-drifting pulsations with the same HF boundary remain noticeable. The main structure here -- the non-drifting spikes in absorption – is the building blocks of all other forms of bursts (see also Figure 9c). Let us note the basic properties of type III-like bursts in absorption we observed.

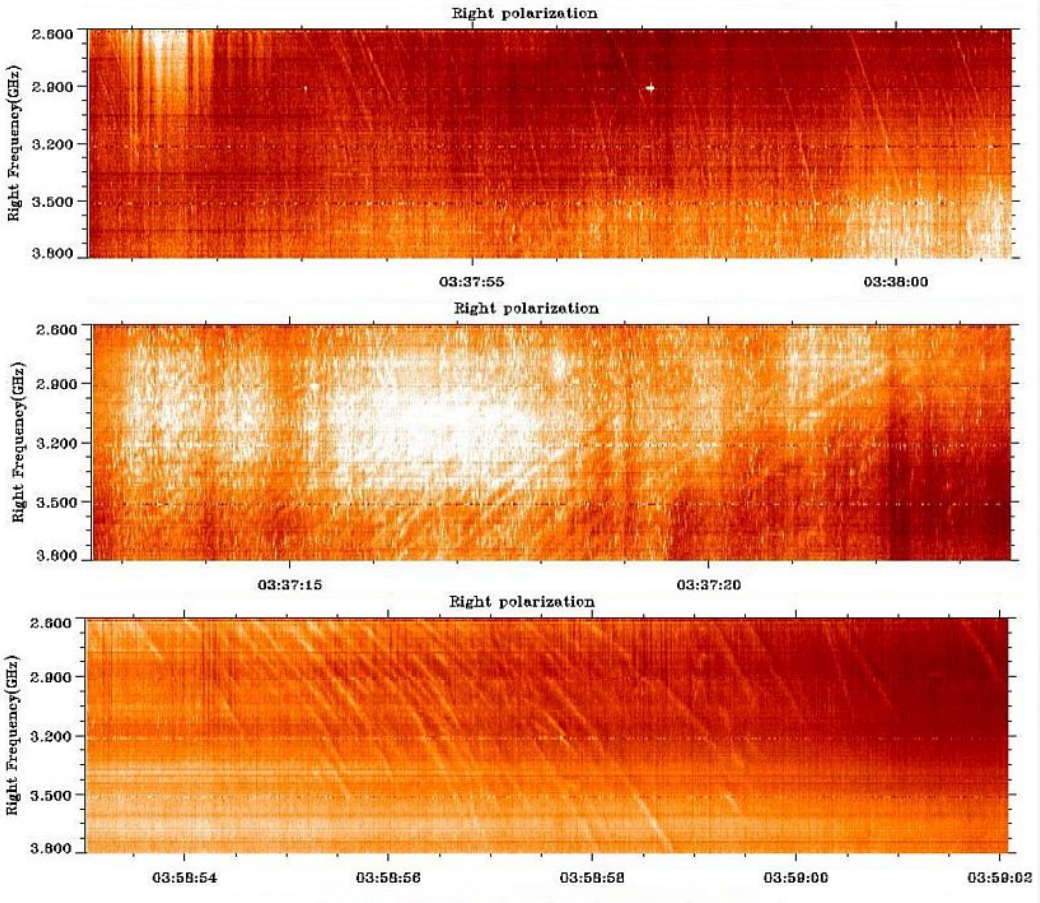

Figure 11 Fiber bursts at the decay phase of the event. In the three panels spikes in emission and absorption are superimposed on fibers or simultaneously visible. The time scales are different in different panels (from Chernov *et al*., 2009).

- The type III-like trajectories consisted of isolated spikes which overlap both in frequency (from the HF part) and frequency separation (from the LF part of the spectrum). These single (broken) trajectories appeared prior to the larger dark type III-like bursts, as well as after them.
- In the large absorptive bursts we were able to count 4-5 sequential trajectories of spikes, which did not show a noticeable frequency-time correlation between them. The drift velocity of type III-like bursts was ≈ -12 GHz s^{-1}.
- In several moments the spikes in absorption in sequential trajectories displaced smoothly to HF, and formed the ZP-like stripes; the maximum duration of stripes was about of 0.12 s in the last burst in Figure 9b. The frequency drift of the stripes was ≈1700 MHz s^{-1}, almost the same as that in the first absorptive ZP-like stripes during 03:29:08 – 03:29:14 UT.

All these details are better visible in enlarged spectra in Figures 12 and 13. Similar short ZP elements drifting like type III burst (or almost vertical columns) are known in the meter range. For example, Slottje (1972, in his Figure 6C) showed numerous almost vertical columns of the ZP. In this case, repeating columns of the ZP can be explained by fast pulsations in absorptions (sudden reductions). Several examples of fast almost vertical columns of the ZP in emission (without sudden reductions) were presented in Chernov (1976b) (see also Figure 19 in Chernov (2006)). Here, we will examine similar fast elements of

the ZP, but in absorption and with much higher time resolution in the microwave range.

Parameters characterizing the observed spikes in emission and absorption are summarized in Table 1. Let us note that the spikes of type 3 have more strictly fixed duration of 8 ms and smaller spread of the frequency bandwidth, and they are repeated strictly through 8 ms.

Table 1 Parameters of spikes in emission and absorption.

Type	Range (GHz) [1])	Duration (ms)	Bandwidth (BW) (MHz)	Relative BW (%)	Period (ms)	Frequency drift
1	0.3 - 1.2	8−16	10−220	0.3 – 7.4	8 → 50	| [2])
2	0.3 - 1.2	8−16	20−400	0.67 – 13.3	8 → 50	|
3	0.3 - 1.0	8	30−160	1.0 – 2.4	8	|
Average absolute error		8	10	0.3	8	

[1]) Frequency range inside 2.6 – 3.8 GHz.
[2]) | - means vertical spikes, the frequency drift approaches infinity.
Type 1 – spikes in emission; Type 2 – groups of spikes in absorption; Type 3 – spikes in absorption as substructures of type III-like bursts.

Five seconds after the absorptive type III bursts (at 03:43:03 UT, a new special feature appeared. The HF boundary of bursts in absorption shifted to lower frequencies, down to 3000 MHz (*i.e.* the radio source must have been displaced upward). Simultaneously, the bursts in emission drifting to HF (or the reverse-drifting type III bursts) with a fixed period ≈ 0.1 s appeared (Figure 9c). Their drift velocity was approximately the same as that in the dark bursts, namely 12 GHz s^{-1}. Then, during almost one minute after 03:43:03 UT the clouds of spikes in emission began to be superimposed on such structures. From Figure 9d, it is evident that at 03:44:01 UT a new property appeared: the HF boundary of type III-like absorptive bursts smoothly displaced to lower frequencies; simultaneously the reverse-drifting bursts in emission stopped at the same frequency boundary; in this case they became less prolonged and more frequent (the period became ≈ 0.03 s).

We note that at frequencies higher than HF boundary, the reverse-drifting bursts continued in absorption and with the period that characterized the reverse-drifting bursts in the emission one minute ago (≈0.1 s). The general appearance of this fragment began to resemble a “herringbone structure” (well known in type II bursts in the meter wave band). The only difference is that it was related to the bursts in absorption. The type III-like burst in absorption and reverse-drifting bursts started at the same frequency, and the starting frequency slowly drifted to the low-frequency region with a drift rate of about –60 MHz s^{-1}. As indicated by Klassen (1996), this could be a signature of propagating bidirectional electron beams originating near the reconnection area. In our event, the reverse-drifting bursts in emission with their starting frequency below 2.6 GHz may indicate the existence of the second site of acceleration above in the corona. At this time (after 03:36 UT), the cusp-shaped flare loop continued to descend (Figure 7), and the activity rapidly changed.

After 03:44:05 UT, the bursts in absorption disappeared together with the HF boundary. The reverse-drifting bursts in emission which covered almost the whole frequency range became dominant bursts. During 03:44:41 – 03:44:44.5 UT the

bursts in absorption reappeared, partially with the fragments of the "herringbone structure". This is shown in Figure 9e, where it is also possible to note that in the end of this interval the reverse-drifting bursts (almost over the entire range) in absorption followed. In the course of the subsequent several minutes after 03:44:45 UT, the bursts in emission and absorption in different combinations with the spikes in emission and absorption still existed. In the course of the last flare brightening (03:55 – 04:05 UT), the bursts in emission (pulsations and spikes) predominated, although the complex forms of bursts in absorption (without type III-like bursts) irregularly appeared.

During 03:58:54 – 03:58:59.2 UT the classical fiber bursts with the reverse drift appeared once more (see the bottom panel in Figure 11). It is remarkable that several stripes of ZP (with the spiky structure) were observed at the higher frequencies (5.2 – 5.7 GHz) at this moment. Thus, in the course of the whole period discussed here, the conditions for the excitation of usual ZP and fiber bursts irregularly appeared. During 04:04:12 – 04:04:20 UT the final series of peculiar slow-drifting stripes, exhibiting different absorption and emission characteristics (as elements of ZP), were observed (the bottom panel in Figure 10).

After 04:05 UT, several small events appeared in the radio emission at 2.84 GHz (Figure 1 in Yan *et al.* (2007)), but the continuum level gradually decreased to the pre-flare level.

2.3.4. Time profiles of bursts in absorption

Figure 12 shows the enlarged spectrum of the sharpest type III-like bursts in absorption at 03:42:56 UT whose duration was ≈ 0.7 s. The intensity profiles at two frequencies (2.85 and 3.06 GHz) clearly show the modulations due to the bursts in emission and absorption. In terms of the absolute scale in the solar flux units (s.f.u.) the maximum flux in emission reached 330 s.f.u. and the minimum flux (in absorption) ≈ 240 s.f.u. with the average level of the continuum of ≈ 280 s.f.u. The maximum of modulation depth at frequency 3.060 GHz was observed between the spike in absorption at ~ 03:42:56.60 UT and the spike in emission 03:42:56.68 (about 80 s.f.u.).

Between the three type III-like bursts in absorption, ZP looks like the classical one (Chernov, 2006): the increased emission in the bright stripes (two high picks on the profiles) and the moderate absorption in the dark ones (here the absorption is even with respect to the average level of flux in the type III-like bursts in absorption). In the spectrum of Figure 12 another property of the usual ZP is clearly seen: the smooth increase with frequency of the frequency separation between the stripes. It increased from ≈ 80 MHz at the frequency of 2700 MHz to ≈ 150 MHz at 3400 MHz.

In the type III-like bursts consisting of isolated spikes in absorption (for example, a trajectory at 03:42:56.3 UT), the instantaneous frequency bandwidth of the spikes also increased with frequency from of 30 to 100 MHz. The decreasing frequency separation between them, disappeared at the frequency of ≈ 3400 MHz. The latter was not coordinated with the frequency separation of the absorptive stripes of the ZP. However, at other onsets noted above for similar bursts this property was not observed.

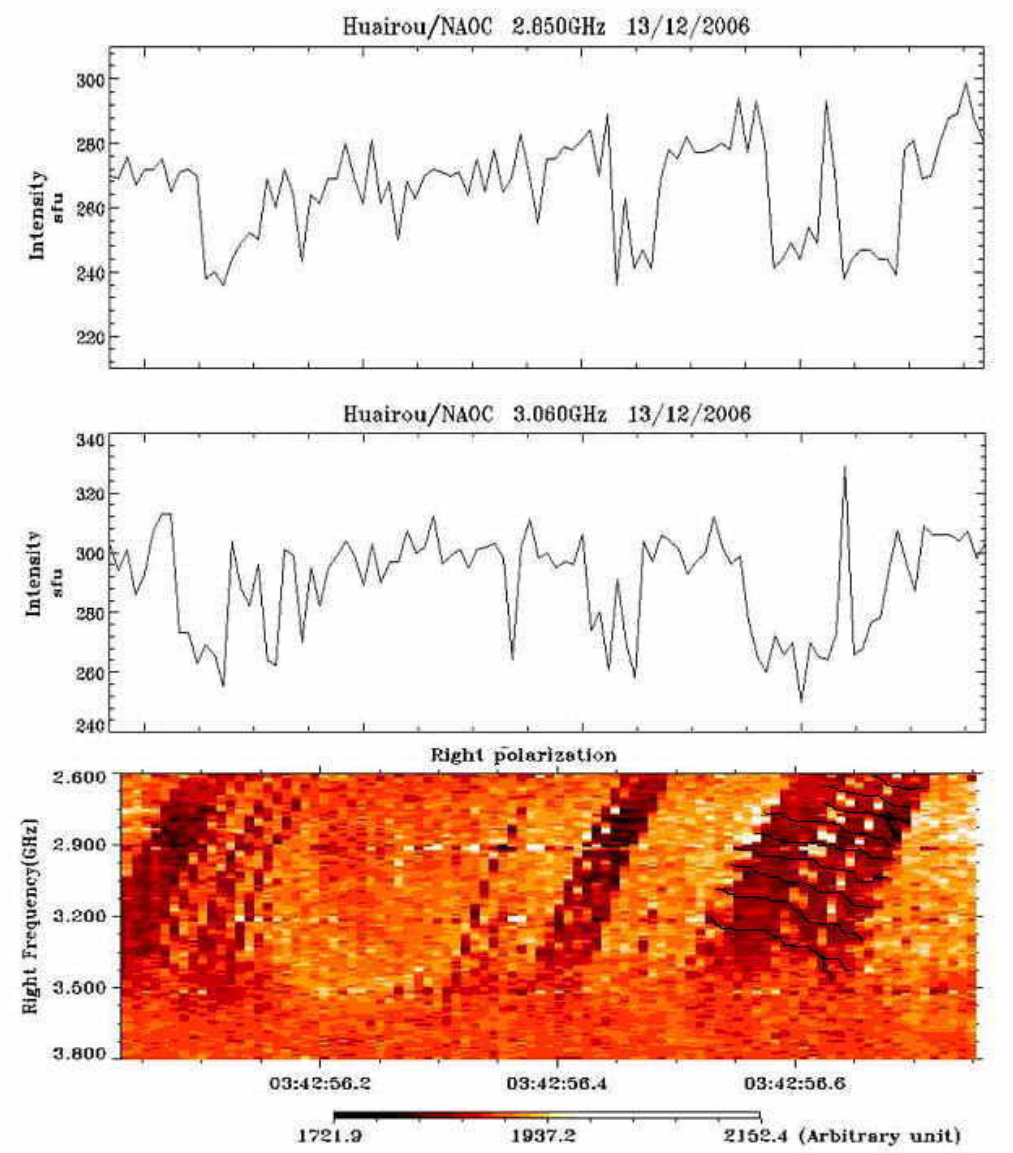

Figure 12 Enlarged spectrum and time profiles at two fixed frequencies (2.85 and 3.06 GHz) of ≈ 0.7 s duration showing the modulations during the type III-like bursts in absorption with ZP. The absorptive ZP-like stripes are marked by thin black lines (from Chernov *et al*., 2009).

The ZP-like stripes appear to be parallel. We can distinguish six stripes against the background of type III-like bursts in absorption (they are marked by thin black lines in the spectrum) and three stripes from the LF edge remained diffuse. However, this conclusion depends on many factors: on the conditions in the radio source and on the rate of particle acceleration in different parts of the radio source. The precise measurements of the frequency drift showed that its speed is also increased with the frequency: from 1000 MHz s^{-1} to 1700 MHz s^{-1}. Thus, it is possible to say that this was a usual ZP, but it was observed against the background of type III-like bursts in absorption. The ZP-like absorptive stripes remained noticeable even against the background of the type III-like absorptive bursts.

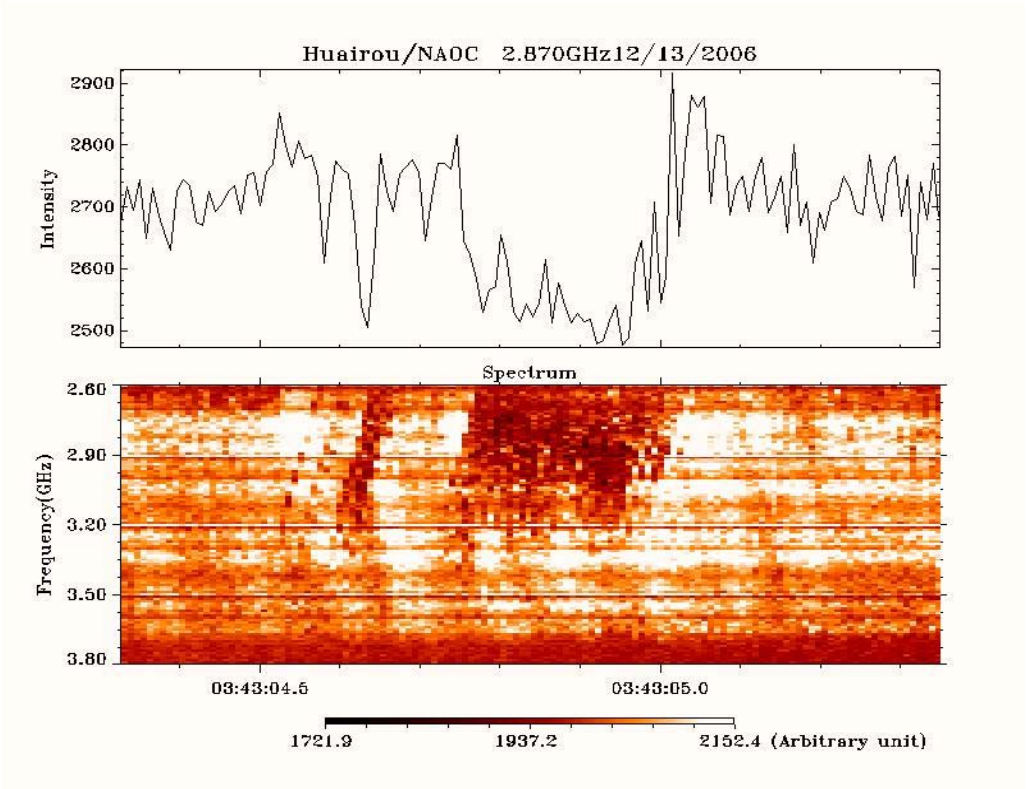

Figure 13 Enlarged spectrum and time profile of ~ 1 s duration at a fixed frequency of 2.87 GHz, showing the modulations during the type III-like bursts in absorption. The intensity scale is in arbitrary units. The spikes, as the substructures of type III-like bursts are clear visible (from Chernov *et al*., 2009).

Figure 13 show the distribution of the spikes in absorption at the background of another type III-like bursts in absorption. The spikes were distributed randomly, but they tended to form several short stripes. Such structures of the spikes were called 'braded ZP' by Slottje (1981) (see the event 27-07-1970) and 'lace bursts' by Karlicky *et al.* (2001) as a variety of the ZP.

Brief Conclusion from Observations

In spite of complexity of the analyzed phenomenon, let us isolate the basic properties of the bursts in absorption.

The basic structural element (a building block) of all bursts in absorption was the spikes whose duration was close to the limit of the instrument resolution (8 ms) and the instantaneous frequency bandwidth was on average of ≈ 70- 80 MHz.

The dynamics of appearance and development of spikes is very rapid. It changed in every several seconds.

The type III-like bursts in absorption were basic structure of the absorptive spikes. In three brief moments, the absorptive spikes created ZP-like stripes which lasted for ≲ 0.1 s.

The complex combinations of the drifting bursts in emission and absorption sometimes exhibited the form of a `herringbone structure.'

The activity of absorptive bursts alternated (or simultaneously observed) with the usual fine structure in emission: spikes, broadband pulsations, ZP and fiber bursts.

This entire interval of the peculiar fine structure was observed during several flare brightenings in the western part of the flare arcade above the south magnetic

polarity. We believe that during this time the probable magnetic reconnection probably took part. The right sign of polarization corresponded to the ordinary wave mode.

The bursts in absorption were sometimes observed in the meter-wave range (Chernov *et al.*, 1998), but the event discussed here for the first time revealed a wide variety of absorptive bursts in the microwave range.

2.4. Other events

Small fibers similar to ones shown in Figure 1 were observed by Dabrowski *et al.* (2005) (Figure 14). However, the authors discuss them as drifting spikes. Dynamical radiospectrograms of the spikes were recorded in the 1352−1490 MHz frequency band split into 46 channels each 3 MHz wide. The time resolution of the collected data is equal to 80 μs, the highest ever obtained. The observations of the radio spikes have been collected with the 15 m radio telescope of Torun Centre for Astronomy, Nicolaus Copernicus University in Torun, Poland. The observed radio spikes have internal structure and form chains (rope-like fibers and braded ZP). They occurred during the bulk motion of the plasma along the long loops, observed with the TRACE telescope in the 171 Å band.

Another kind of spikes (called as dot emissions) was observed with Brazilian Solar Spectroscope (Meszarosova *et al.,* 2008) in dm range of 950−2640 MHz with variable time and frequency resolution between 10−1000 ms and 1−10 MHz, respectively. An example of a group of dot emissions arranged as zebra-like chains observed on March 19, 1999 is shown at Figure 15 (as a part of Figure 1 from Meszarosova *et al.* (2008)). Panel *b* presents a global view of the dot emissions. The time and frequency resolution is 100 ms and 5 MHz, respectively. Panel *c* reveals a detailed view showing the dot emissions with undulating chains resembling the zebra pattern. Panel *d* shows the radio flux in time at 1400 MHz where peaks with an intensity of ~ 130 SFU correspond to individual dot emissions (horizontal line in panel *c*).

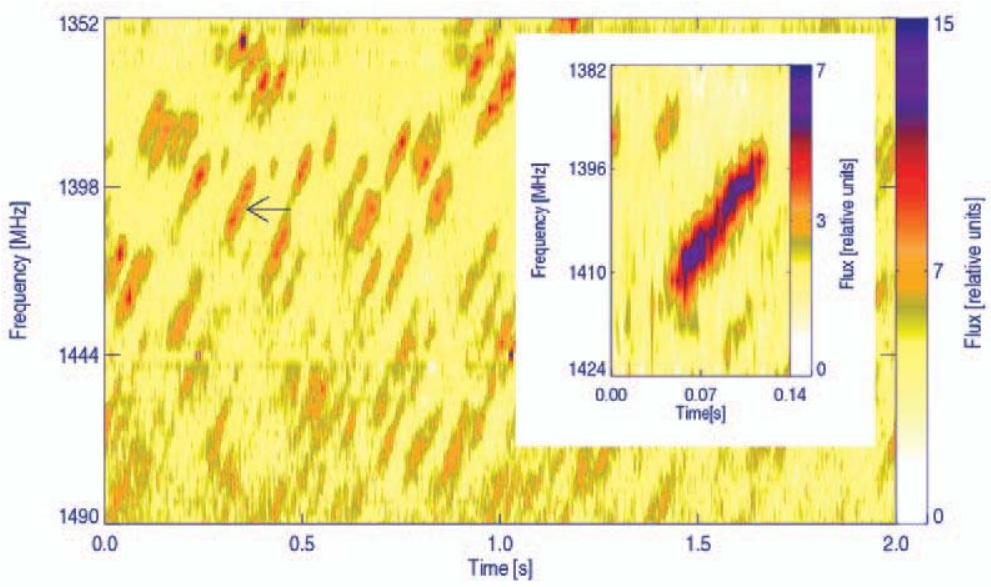

Figure 14 Dynamic radiospectrogram of the dm radio spikes recorded on 30 October 2001, beginning at 12:20:27 UT (from Dabrowski *et al.,* 2005).

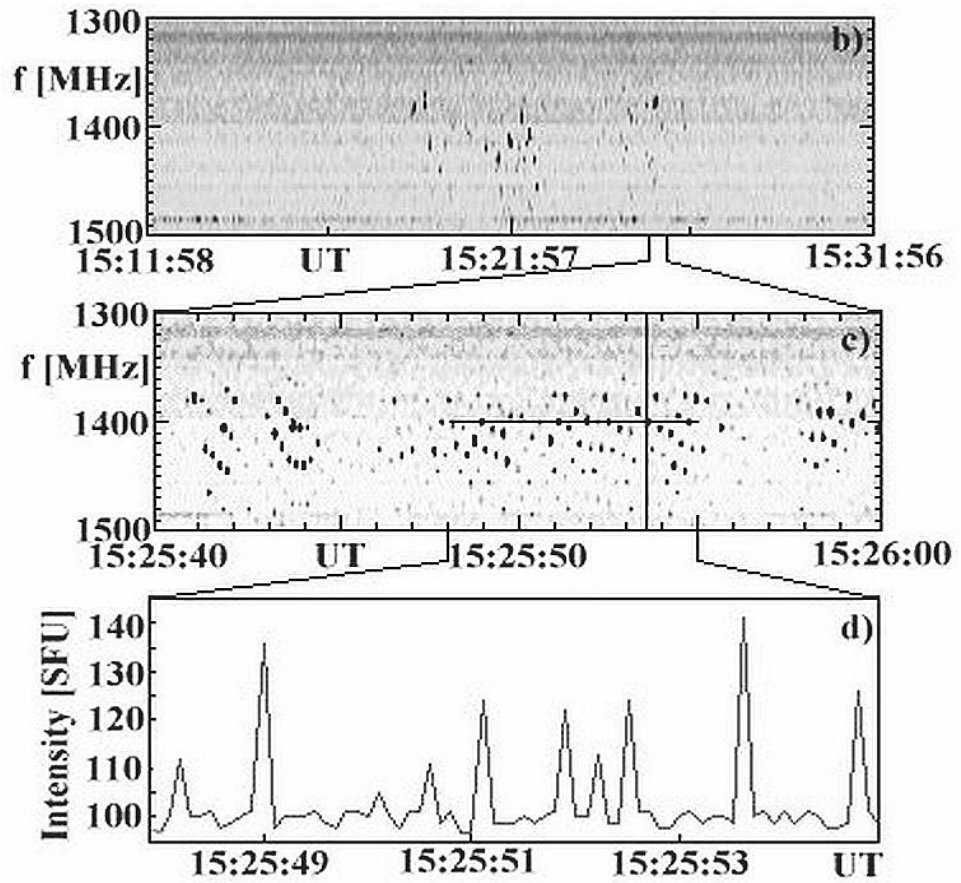

Figure 15 Dot-emissions (in black) arranged as zebra-like chains observed on March 19, 1999: *b*) global view of dot emissions, *c*) zebra-like chains, *d*) radio flux in time at 1400 MHz (horizontal line in *c*) (from Meszarosova *et al*., 2008).

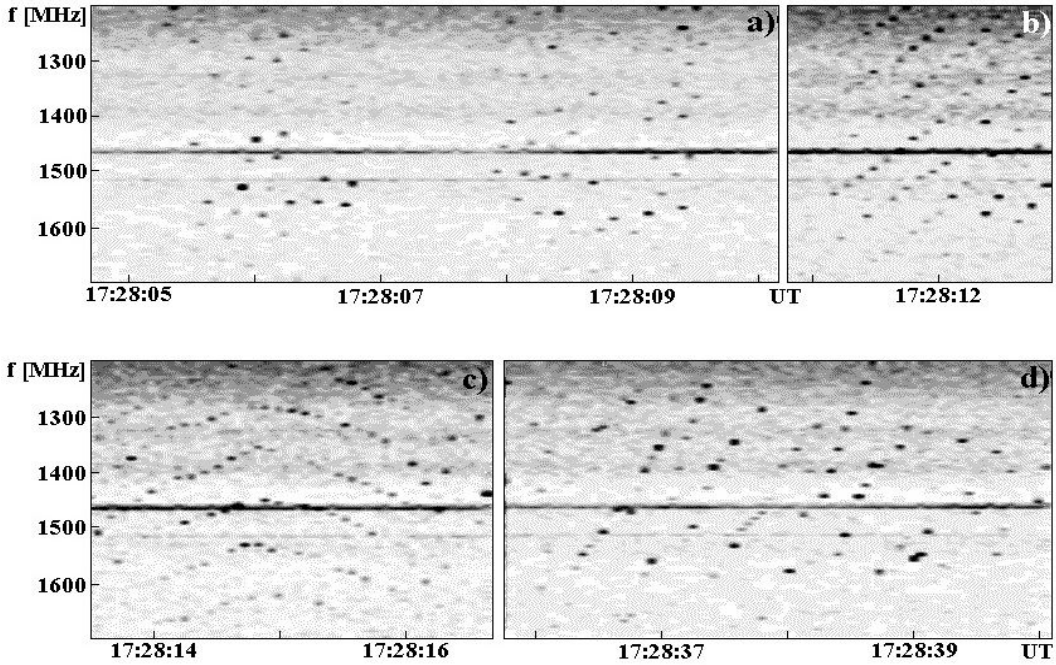

Figure 16 Example of the arrangement of series of the dot emissions (in black) observed on October 19, 1999: irregular dot emissions (panel *a*)), fiber-like chains (panel *b*)), zebra-like chains (panel *c*)), and irregular dot emissions (panel *d*)) (from Meszarosova *et al*., 2008).

Figure 16 shows an example of structural evolution of the group of the dot emissions observed on October 19, 1999. This group starts with some irregular dot emissions (panel *a*) but later they evolve into almost regular fiber-like (panel *b*) and zebra-like (panel *c*) chains. At the end the group of dot emissions again become irregular (panel *d*). At times of dot emission no background burst emission was detected.

Sych *et al.* (2006) and Zlobec and Karlicky (2008) studied the characteristics of the zebra-associated spike-like bursts during 5 August 2003 event that were recorded by the Ondr˘ejov radio spectrograph in the range 1 – 2 GHz with time resolution 100 ms (upper panel in Figure 17). Simultaneously, the spiky structure was examined using the 1420-MHz polarization profiles of the Trieste Astronomical Observatory with very high time resolution of 1 ms (bottom panel in Figure 17). The selected spike-like bursts show a duration (with a mean value of about 7.4 ms at half power) and it is not influenced by the polarization. For the selected bursts there was just a "tendency" that the weaker component (L-polarization channel) should be delayed. Zlobec and Karlicky (2008) realized that the L continuum was generally low with respect to the R continuum; however, the polarization of the spikes do not always match the contemporaneous polarization of the continuum.

The observed superfine structure (spikes) of zebras can be interpreted as proposed by Chernov, Yan, and Fu (2003). Nevertheless, Zlobec and Karlicky (2008) think that the model based on the double plasma resonance (DPR) as proposed by Bárta and Karlický (2001) and Karlický *et al.* (2001) is also possible. Namely, this model explains both the zebras and the spikes by the same double plasma resonance process; the spikes are generated by the interruption of the DPR process by assumed turbulence (density or magnetic field variations).

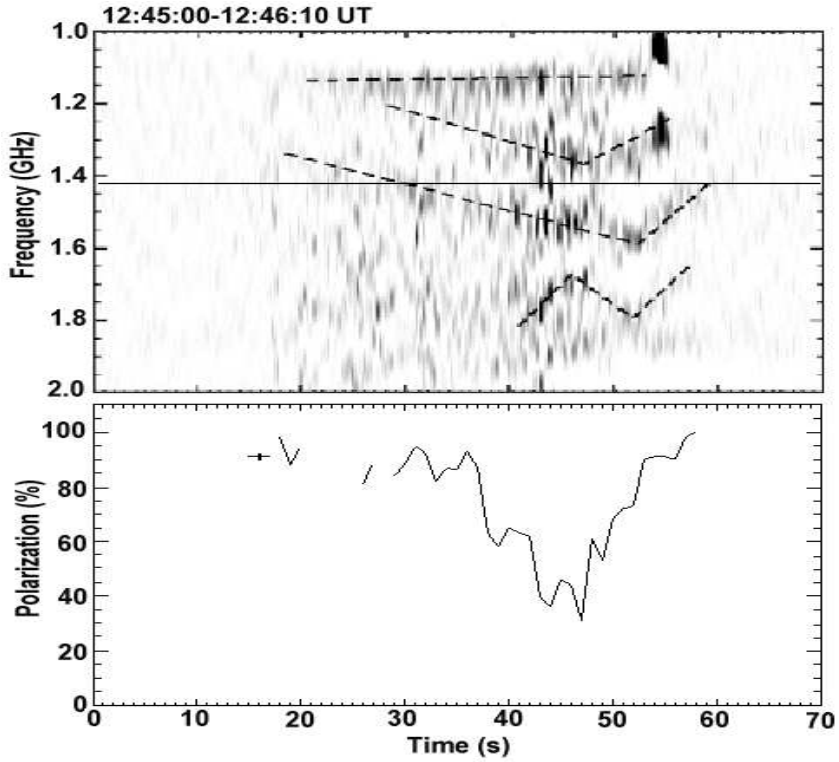

Figure 17 *Upper panel*: Part of Figure 5 from the paper by Sych et al. (2006) showing the time evolution of the spike-like bursts clustered into zebras forming "V" like structure (in the event August 5, 2003). *Bottom panel*: contemporaneous time evolution of the mean polarization (in R-sense) of the selected spike-like bursts at 1420 MHz (from Zlobec and Karlicky, 2008).

Magdalenic' *et al*. 2006 reported about supershort structures SSSs (spikes), in particular as substructure of ZP and as tadpoles in the range 265 – 350 MHz using the solar radiospectrograph Artemis IV (Greece) with time resolution of 10 ms (Figure 18). The spikes in ZP exhibit duration of 11 – 13 ms, shorter than it was reported earlier in the meter range. Tadpoles are comprised of an emission "eye" with a duration of ≈ 50 ms at the high-frequency side of the burst and a stretched absorption "body" with a bandwidth of ≈ 40 MHz. In spite of distinctive differences (the emission tail of tadpoles is not visible), the Slottje (1972) tadpoles and these tadpole-like SSSs belong to a class of physically equivalent bursts.

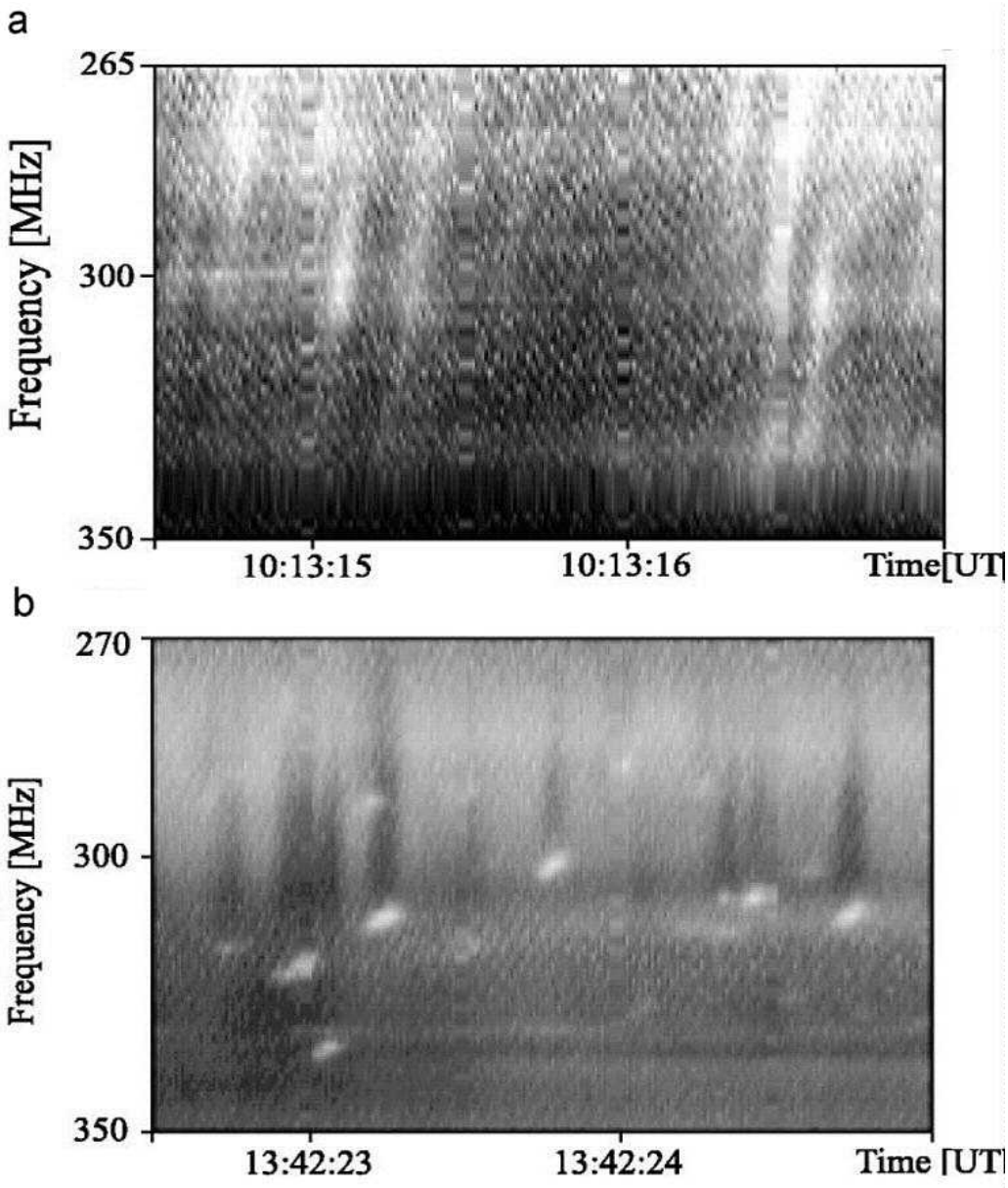

Figure 18 Artemis IV dynamic spectra of negatively drifting supershort structures (SSS) at the background of ZP with a superfine structure (*a*) and tadpole-like bursts (*b*) in the event April 15, 2000 (from Magdalenic' *et al*. 2006).

3. General Discussion of the events

24 July and 3 November 2004 events

Small-scale fibers differ from usual fiber bursts only by narrow total frequency bandwidth and they are similar to ropes of fibers, therefore the usual (the most accepted) mechanism for fiber bursts should work, namely the coalescence of plasma wave (l) with whistlers (w): $l + w \rightarrow t$ (Kuijpers, 1975b; Chernov, 1976a; 1990). However, the propagation of whistlers is limited by a small magnetic trap in the form of fast shock fronts escaping from a region of the magnetic reconnection (Chernov, 1997). In our case a periodicity of fibers was not so evident, and fibers were organized as large-scale stripes of ZP. So, these ZP stripes become visible only when whistlers propagate through the ZP source.

More than ten different models have been proposed for ZP, most of them including some emission of electrostatic plasma waves at the double plasma-resonance (DPR) frequency (Kuijpers, 1975a; Zheleznykov and Zlotnik, 1975; Mollwo, 1983; 1988; Winglee and Dulk, 1986; Chernov, 2006) :

$$\omega_{uh} = (\omega^2_{Pe} + \omega^2_{Be})^{1/2} = s\omega_{Be} \qquad (1)$$

where ω_{uh} is the upper-hybrid frequency, ω_{Pe} is the electron plasma frequency, ω_{Be} is the electron cyclotron frequency, and s is the integer harmonic number. The model which in the best way describes the observations and the conditions in the corona is the one by Winglee and Dulk (1986), which is based on unsaturated electron-cyclotron maser emission by electrons with a loss-cone distribution.

In our events the radio sources cannot be point-like ones, since in such a case one whistler wave packet should produce all zebra stripes simultaneously, but we did not see such a feature. Since the small fibers were not connected by a unique straight line in the dynamic spectra, we cannot assume that one whistler wave packet passes through several DPR levels consecutively in an extensive source. So, the unique possibility remains that whistlers are excited at the same DPR level simultaneously with the plasma waves. Without whistlers, ZP stripes cannot be visible, at least in the DPR model with loss-cone distribution function, in accordance with numerical results of electrostatic instability in Kuznetsov and Tsap (2007). Whistlers without plasma wave cannot be detected either, but a plasma wave of low energy will be sufficient (at places of DPR) to emit radio waves of sufficient intensity. Thus, whistlers "highlight" DPR levels.

In order to confirm this hypothesis, let us estimate the magnetic field strength B in two ways. One is from the observations of separate fibers using the model on the whistlers, and the other is from large-scale ZP in the DPR model. If the hypothesis is correct, these values of the field strengths should be equal.

From the whistler model for small fibers we have $\Delta f_e \approx f_w \approx 0.1\, f_{Be}$ (f_w is the whistler frequency), and a mean value $\Delta f_e = 12.5$ MHz (for the events of 24 July and 3 November), and we obtain $B \approx 45$ G.

In the DPR model the frequency separation depends on the scale heights of density (N_e) and magnetic field ($L_{Ne} = 2N_e\, (dN_e/dr)^{-1}$ and $L_B = B\, (dB/dr)^{-1}$ (Zlotnik *et al.,* 2003):

$$\Delta f_s / f_B \approx L_B / |L_{Ne} - L_B| \qquad (2)$$

For $\Delta f_s = 72$ MHz (for 3 November event) we could obtain about the same value $B = 46$ G for $L_{Ne} = 1.4 \cdot 10^9$ cm and $L_B = 5 \cdot 10^8$ cm. In the flare region the plasma is

very inhomogeneous and such scale heights are realistic. In our events only 3 – 4 large-scale stripes of ZP (or DPR- levels) are simultaneously formed in the spectrum that demonstrates the small sizes of local L_{Ne} and L_B in flare inhomogeneities. Four DPR levels are simply realized at harmonic number s = 10 – 14 with such a ratio of scale heights.

The stable frequency drift of fibers implies that the magnetic field changes little during the lifetime of the structure (Chernov, 1990). The frequency drift of fibers is mainly determined by the group velocity (υ_{gr}) of whistlers, and we have $\upsilon_{gr}=2c\times f_{Be}/f_{Pe}\times [x(1-x)^3]^{1/2}$, where $x=f_w/f_{Be}$ is the ratio of whistler frequency to cyclotron frequency (Kuijpers, 1975a). If we assume the parameter x varies little during the lifetime of the structure, and f_{Be}/f_{Pe} has a consistent value due to DPR condition, then υ_{gr} would vary little and consequently the whistlers would cause a stable frequency drift of fibers, at least within a certain DPR level. Therefore the positive frequency drift of large-scale ZP can be connected with the downward motion of the source. In the absence of a good analytical model of electron concentration in the upper chromosphere, we will use a graphical representation given, for example, in the model of Allen (in Figure IV.1 of Krüger (1979)). Passing to the dependence of plasma frequency (f_{Pe}) on the height (r), it is possible to roughly estimate the value of the gradient of f_{Pe} between 1000 and 2500 MHz on the order of 240 MHz/10^8 cm. Then, we can use the simplest expression for definition of the velocity of propagation:

$$V \approx 2\frac{df/dt}{f}\frac{N_e}{dN_e/dr} = \frac{df/dt}{df_{Pe}/dr} \quad . \qquad (3)$$

And the frequency drift df/dt = 630 MHz s^{-1} will correspond to the velocity of about 2590 km s^{-1}. Such a value might be more than a typical Alfvén velocity. Therefore it is possible to assume that the plasma ejection that moves downward from the magnetic reconnection region has caused a shock wave.

In the 24 July event the drift of 220 MHz s^{-1} implies the velocity ≈ 900 km s^{-1} which is somewhat more than the Alfvén velocity (V_A ≈ 700 km s^{-1} for the estimated value of B = 45 G).

The drifting boundary of the emission termination at high frequency edge of large-scale ZP may mean that a moving shock front meets a rising closed magnetic loop. So, the conditions for DPR are realized only in a narrow height interval, below of the magnetic reconnection region, and only at the very beginning of events. After such a collision they will be destroyed, and large-scale zebra stripes will be transformed into braided ZP (Figures 1b). Thus, the radio source showing such a fiber structure differs from the radio source of the rope of fibers only by the absence of a magnetic trap (only one shock front) where fast particles could make periodic bounce motions, and by short living conditions for DPR. The absence of any absorption is simply explained by the absence of continuum emission at the very beginning of events. Only the pulsations in the 31 October event were observed against a weak continuum, and we could detect some fragments of absorption between fibers (Figure 6 in Chernov *et al.* (2008)).

Thus, we assume that the usual mechanisms can be applied for the interpretation of such a fiber structure: the coalescence of whistler waves with plasma wave for fiber bursts and DPR- model for large-scale ZP. However, the following special features of the plasma wave excitation in the radio source must be present. Both whistler and plasma wave instabilities are too weak at the very beginning of the events (the continuum is almost absent), and the fine structure is

almost invisible. Moreover, according to the recent simulations of Kuznetsov and Tsap (2007) the fast electrons with loss-cone distribution cannot excite high enough level of electrostatic waves at the DPR levels, so that the separate stripes would be visible. Then, whistlers generated directly at the DPR levels by the same fast electrons will "highlight" the radio emission only from these levels due to the interaction with plasma waves and we observe small-scale fibers as a substructure of ZP. More precisely, the whistler packets may bring about sufficient plasma wave energy as well as new composition of particle distribution, therefore the DPR levels could be more pronounced and "highlighted".

Wu *et al.* (2007) are interpreted the small-scale fibers in the 3 November event as drifting spikes emitted from "solitary kinetic Alfvén waves" (SKAWs) by fast electrons accelerated by the electric field and trapped in SKAWs. However, they did not discuss the reasons for the formation of fibers along the stripes of large-scale ZP. Furthermore, the source of the strong Alfvén waves, which accelerate a large fraction (≈ 0.1) of the background electrons at the beginning of the event also was not examined.

We have not adopted the model of LaBelle *et al*. (2003), since it is supposed to be applied to the explanation of a large number of stripes with the narrow frequency separation. In large-scale ZP in question, on the contrary, the frequency separation is considerably wider than in the usual ZP. Recent evaluation by Chen and Yan (2008) on the validity of the mechanism of LaBelle *et al.* (2003) indicated that, with the realistic values of the density contrast (of $\delta \leq 0.2$) the model cannot account for a large number of ZP stripes.

However, we cannot completely exclude the possibilities of the application of the new models, based on the existence of the bands of transparency and opacity when the radio waves propagate through spatially periodic medium (for example, Laptuhov and Chernov, 2006). It is possible that the large-scale ZP is the result of this selectivity with the specific scale of thermal heterogeneities, which move downward from the flare region, and small-scale fibers are caused by additional quasi-periodic modulation of these heterogeneities, for example, by a fast magneto-sonic wave propagating from below. Or alternatively and more simply, the radio waves meet on their way the small- and large-scale heterogeneities which move toward different directions, *i.e.* a radio wave is filtered by transparency bands twice. These possibilities require more detailed study.

Considering all aspects of the observed dot emissions, Meszarosova *et al.* (2008) think that the dot emissions are generated in a similar way as zebras (Ledenev et al. 2001) or lace bursts (Karlický et al. 2001). Thus, they propose that the dot emissions are produced in the solar atmosphere at the locations where the so-called double plasma resonance condition (1) is fulfilled. The upper-hybrid waves at these locations can be generated e.g. by the anisotropic beam ($T_\perp > T_\parallel$, where $T_\perp$ and $T_\parallel$ are the temperatures of energetic electrons across and along the magnetic field, respectively) accelerated during the flare primary energy processes. The beam anisotropy can be naturally formed along magnetic field lines by an escape of fast electrons from slower ones. Then these upper-hybrid waves are transformed to electromagnetic waves (with the frequency $\omega_{el} \approx \omega_{uh}$ or $\omega_{el} \approx 2\omega_{uh}$), which are observed by radiospectrographs on the Earth. This process is a resonant one which means that its intensity can be several orders of magnitude higher than those associated with non-resonant processes. This can explain the fact that at times of dot emission no background burst emission was detected.

Using this model we can explain not only individual dot emissions, but also their chains. The beam along its trajectory generates dot emissions in several resonance locations (*s*-harmonics). The higher *s* means a higher height of the dot emission source in the solar atmosphere. Thus fiber-like chains of the dot emissions can be formed. On the other hand, zebra-like chains of the dot emissions can be explained by a sequence of anisotropic beams producing dot emissions nearly at the same position on the same *s*-harmonic. Even the whistler waves, which are considered in the model of fibers, can enhance emission at the locations with double resonance conditions. Therefore both forms of zebra-like and fiber-like chains are possible.

Due to similarities in morphology and characteristic properties between the dot emissions and dots in fine structures of zebras and fibers, Meszarosova *et al.* (2008) think that both have a similar physical origin. They found that fiber-like chains of the dot emissions evolve into zebra-like chains and vice versa. These changes are in agreement with the idea of Chernov *et al*. (1998) who proposed that both the zebras and fibers are generated by whistler packets. The propagating whistler packets may also generate dot emissions at the positions in the solar atmosphere where the double resonant conditions are fulfilled (see also, Sawant et al. 2002; Krishan et al. 2003). Furthermore, they propose that the chaotic character of some groups of the dot emissions is due to rapidly varying plasma parameters (in the MHD turbulence) in the region of the dot-emission sources.

13 December 2006 event

From the observations discussed above in detail, we are able to understand the reason for the appearance of the spikes in absorption, as well as the variable nature of their parameters. The main task is to explain formation of the absorptive type III-like bursts and absorptive ZP-like stripes of the absorptive spikes, in combination with different bursts in emission.

Let us recall that the loss-cone instability is the most probable mechanism of the continuous radio emission of the type IV bursts (including microwave bursts). Plasma waves are excited at the upper hybrid frequency by the fast electrons, captured in a magnetic trap, where the particle-velocity distribution with the loss-cone is formed (Stepanov, 1974; Kuijpers, 1975a; Zhelezhyakov, 1995; Kuznetsov and Tsap, 2007). The maximum amplification of waves occurs under the conditions of double plasma resonance (DPR, when the upper hybrid frequency is close to integer harmonics of the electron cyclotron frequency). The appearance of usual ZP and fiber bursts during the entire event attests to the fact that the loss-cone velocity distribution actually existed.

The dips in emission (corresponding to bursts in absorption) mean the quenching of the loss-cone instability. According to Zaitsev and Stepanov (1975), Benz and Kuijpers (1976), and Fleishman *et al.* (1994), this quenching can occur because of additional injection of fast particles, which fill the loss-cone. The process of the quenching of instability is examined in detail in a recent paper by Chen and Yan (2008). The authors showed (Figure 17) that the beam with a linear dimensions of ≈ 220 km and a Maxwellian particle-velocity distribution inside the loss-cone causes absorption with frequency bandwidth of ≈ 60 MHz (due to the cyclotron self-absorption of upper-hybrid waves). The calculated absorptive depth corresponds to the observed value: the modulation in the growth rate in Figure 17 corresponds exactly to the observed absorption depth of ≈17% in our Figure 12. Let us note that according to the calculations by Kuznetsov and Tsap (2007), the

beams with the power-law spectrum with a large spectral index should give bursts in emission (the spiky superfine structure of the ZP stripes).

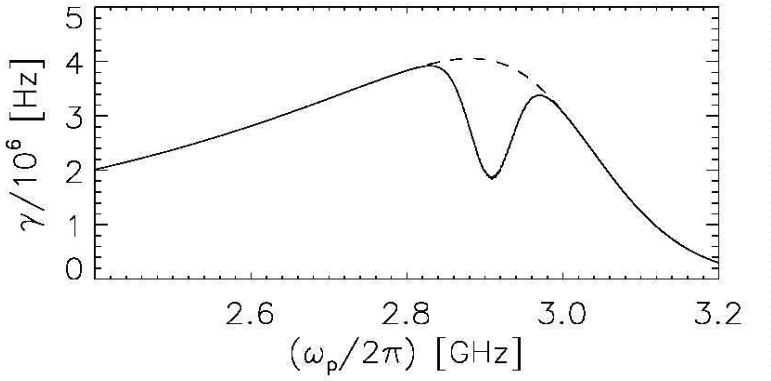

Figure 17 Dependence of the total growth rate γ of the upper hybrid waves on the plasma frequency. The initial growth rate result corresponds to a value of s = 15. Signs of an absorption feature with a frequency bandwidth of about 60 MHz can be clearly seen (from Chen and Yan, 2008).

Taking into account the fact that absorptive spikes do not always follow along the type III trajectories, and that they are often a random collection of instantaneous bursts, it is natural to assume a random acceleration of small-scale beams. The dimensions of beam would then determine the instantaneous frequency band. The quenching of instability occurs only when the instability develops in the location of the beam. Then the beam rapidly leaves the region, and the emission will be restored there. Most likely, the maximum effect is achieved in the DPR conditions. Therefore, when the moving beam reaches a neighboring DPR- level, a certain space between the spikes in absorption will be formed. By this method, it is possible to explain the discrete nature of absorptive spikes. Various parameters of the absorptive spikes can be associated with different local gradients of density and magnetic field. At the beginning of the interval of bursts in absorption, the spikes in absorption were still accompanied by spikes in emission with the similar parameters (Figure 8a). It means that at this moment not all beams were seized into the trap. This untrapped part of the beams would have given bursts in emission, although the beams did not move ahead further, possibly, they were reflected.

In the mildly inhomogeneous corona, the DPR- levels are the surfaces whose the size perpendicular to the line of sight is more than 10,000 km. Compared to this size, the magnetic loops are very narrow and inhomogeneous in density, so that the DPR- levels in the adjacent loops cannot coincide with each other. If the beams of particles were periodically injected along one loop, then we should always see ZP. Therefore, most likely they are injected consecutively in time and simultaneously in several loops. In cases like this, we would often observe almost random distributions of spikes in the type III-like bursts (Figure 13). But if the DPR- levels almost coincide among the adjacent loops, then a smooth displacement of dark spikes would be realized, and at these moments the ZP will appear. The frequency drift of the ZP- stripes ($\approx$ 1700 MHz s^{-1}) can be explained by an appropriate displacement of the DPR- levels in the corona. Even a slow downward motion of a loop making a sharp angle with respect to the gradient of plasma frequency (which exactly occurred, according to the TRACE images in Figure 7) could lead to rapid lowering of DPR- levels in the corona, which will also explain the frequency drift of ZP stripes. During the resistive tearing-mode instability (see below), the condition of frozen magnetic flux is disrupted, and

magnetic field line can move independently of the plasma (Aschwanden, 2004, p. 414).

The beam traveling between the DPR- levels can give impulsive contributions to the emission on the Cerenkov resonance, so that the appearance of bright ZP stripes (spikes in emission) is entirely expected (the plasma mechanism of type III bursts). The frequency drift of type III-like absorptive bursts ($\approx$ 12 GHz s^{-1}) would correspond to the speed of the electron beam not exceeding of 10^{10} cm s^{-1} in accordance with Allen's density model of the corona (see Fig. IV.1 in Krüger (1979)).

Wang *et al.* (2008) considered that the spikes in emission are generated by the electron cyclotron maser (ECM) mechanism. However, the majority of spikes with right circular polarization were observed during flare brightening in the northern flare ribbon in the South magnetic polarity. Thus, the radiation mode was ordinary. Two episodes with left circular polarization were connected with the brightening in the southern flare ribbon (see the black rectangle in Figure 3b of Wang *et al.* (2008)) where the North magnetic polarity could be dominant. This means also the ordinary wave mode, while in the ECM radiation the extraordinary mode should dominate (Fleishman and Melnikov, 1998). For this very reason the estimations of the magnetic field strength obtained by Wang *et al.* (2008) in the ECM model exceed almost by an order of magnitude the ones obtained by Yan *et al.* (2007) using the frequency separation of ZP stripes.

The simultaneous presence of bursts in emission and absorption with different drift rates (Figure 9c and 9d) testifies that at least two places of particle acceleration exist at the different heights. In accordance with Figure 7 (the pictures at 03:23 and 03:36 UT) we can assume that above the cusp-loop, in the course of the post-flare restoration of magnetic structure a magnetic island was probably formed, and particle acceleration occurred in the two current layers located above the flare cusp-loop (upward) and above the magnetic island (downward). Such an assumed scheme coincides with the sketch of magnetic configuration proposed for this flare in Figure 8 in Guo *et al*. (2008).

As Schwenn *et al*. (2006) diligently noted, despite many decades of indirect observations suggesting the presence of a current sheet, such as soft X-ray cusp structures (Tsuneta, 1996) and horizontal inflow, direct observations of the formation and evolution of a current sheet in the solar atmosphere have been missing. Strong observational evidence for reconnection comes from the post-eruption emission and dynamics. Our radio observations also testify to the probable case for reconnection in the erupting solar corona.

The rise of helmet-shaped loops in three TRACE images at 03:02, 03:20 and 03:23 UT in Figure 7 allows us to propose the existence of a single X- point above the helmet-shaped loop, and the initiation of flows due to the magnetic reconnection. The consecutive flows may be associated with the formation of magnetic islands above the helmet loop. The sketch of the magnetic configuration can be similar to Figure 8 of Pick *et al.* (2005) as a two-dimensional cut of the three-dimensional configuration across the twisted flux rope. Similar two-dimensional magnetic configurations were often discussed in many numerical simulations (Tsuneta, 1996, Lin and Forbes, 2000, Aschwanden, 2004, and references herein). The three-dimensional flux rope is in fact anchored (line-tied) to the photosphere. The theory of three-dimensional reconnection is presented in greater detail in the book of Priest and Forbes (2000). The two-dimensional representation is mostly done for convenience, but the magnetic structure is three-dimensional (see Figure 4 in Roussev *et al.* (2003) for a view of very complicated

magnetic field configuration). All special features of two-dimensional reconnection enumerated in Pick *et al*. (2005), are also valid in our case. In the framework of an erupting flux rope, magnetic reconnection occurs behind the twisted rope. The accelerated particles form beams along the newly reconnected field lines and propagate both upward and downward.

Two places of acceleration, separated in height suggest the tearing-mode instability, in that two (or more) magnetic islands were formed and the entire activity at the post-eruptive phase is associated with the restoration of the magnetic structure.

The analysis of microwave pulsations by Tan *et al.* (2007) confirms such an evolution of the flare. They concluded that the flaring region consisted of many current-carrying compact loops. In each current-carrying flare loop, the resistive tearing-mode instability will trigger the formation of a series of multi-scale magnetic islands. The X-point is located between the two magnetic islands. The opposite frequency drifts of pulsations also suggest the particle acceleration in the opposite directions.

The radio bursts drifting in the opposite directions in the frequency coverage of the spectrograph (Figures 5c and 5d) indicate the simultaneous existence of two places of particle acceleration in the current sheets between the magnetic islands. The fast particles moving from the higher to the lower corona are responsible for the type III burst in emission with the reverse drift. The fast particles moving from the lower to the higher corona are seized in the magnetic trap and give the type III-like bursts in absorption with the negative drift.

Karlicky and Barta (2007) found that electrons are accelerated most efficiently in the region near the X-point of the magnetic reconnection at the end of the tearing process and the beginning of the restoration of the magnetic configuration. In this connection, all intervals of new peaks in burst profile at the decay phase (Figure 1 in Yan *et al*. (2007)) were very rich of spikes in absorption, type III–like bursts consisting of spikes in absorption and usual ZP and fiber bursts with different frequency drift (see Figures 8–11). The appearance of ZP and fiber bursts means the existence of the loss-cone velocity distribution of fast particles inside the radio source (magnetic islands).

The beams, accelerated above flare loop would have propagated upward and fallen into the magnetic trap, where the loss-cone distribution of fast particles was already there, and would have caused bursts in absorption. The particles accelerated above the magnetic island would have probably propagated along the overlying magnetic loops downward (where the loss-cone distribution was absent). They might have produced simultaneously the reverse-drifting bursts in emission. The comparison of spectra in Figure 9b – 9d suggests a slow lift of the lower site of particle acceleration, which may have created a kind of `herringbone structure'. After ≈ 03:44:01 UT the reverse-drifting bursts in emission stopped by the drifting boundary (a hump of the `herringbone structure'). At higher frequencies their continuation transformed to bursts in absorption (though their relationship is not very clear). The loss-cone distribution was probably formed there up to this moment and the quenching of instability by additional beams became already as the main effect.

The difference in the parameters of these bursts in absorption (they were prolonged, broad-banded and diffuse) indicates that these beams were larger in scale and their velocity dispersion was wide (≈1). The velocity dispersion in the beams, critical for the spikes in absorption, was much less than 1. New beams with great longitudinal velocities stimulate the whistler generation at the

anomalous Doppler resonance and as a consequence, the formation of ZP stripes in emission (in Figure 12 at 03:42:56 UT) could be explained in the whistler model (Chernov, 1996).

When the slowly drifting boundary became almost indistinguishable at 03:44:44 UT, the diffuse reverse-drifting bursts in absorption covered the whole frequency range (2.6 – 3.8 GHz), and the spikes in absorption almost disappeared. Up to this moment, the existence of magnetic island must have ended.

4. New theories of ZP

4.1. WHAT IS NEW IN IMPROVED DPR-BASED ZP THEORIES?

The mechanism proposed in LaBelle *et al.* (2003) can be regarded as an important step in attempts to improve the DPR-based model. The escape of the Z mode is considered at one DPR level (a point radio source), whereas the harmonics are assumed to be eigenmodes that penetrate through regular inhomogeneities, such as an ion-acoustic wave. The number of harmonics is large only if density variations in the ion-acoustic wave reach ~20%. However, as was shown in Chen and Yan, (2008), it is hardly possible that such a strong ion-acoustic wave be generated in the solar corona; in fact, the amplitude of density variations is no more than ~2%. In this case, only several ZP stripes can be generated by this mechanism, whereas up to a few tens of stripes are usually observed. In our opinion, a disadvantage of this theory is that it fails to explain the high intensity of radiation emitted by separate incoherent sources.

In the basic papers on the DPR theory (Zheleznyakov and Zlotnik, 1975; Winglee and Dulk, 1986) the velocity distribution function of fast particles was assumed to be narrow, with an infinitely small spread in velocities; therefore, calculations of the growth rates of upper hybrid waves could hardly provide a realistic picture (Chernov, 2006). Besides, Winglee, and Dulk (1986) restricted themselves by consideration of the Maxwellian distribution of particles over momentum that could significantly affect the results obtained. This was clearly demonstrated in Kuznetsov and Tsap (2007), where the following electron distribution function of the loss-cone type was chosen (see Figure 18):

$$f_p(p,\theta)=\varphi(p)\begin{cases}0, & \theta \le \theta_c-\Delta\theta_c \\ \dfrac{\theta-\theta_c+\Delta\theta_c}{\Delta\theta_c}, & \theta_c-\Delta\theta_c<\theta<\theta_c, \\ 1, & \theta>\theta_c\end{cases} \qquad (4)$$

where the function $\varphi(p)$ describes the electron distribution over momentum and θc is the loss-cone boundary with a width $\Delta\theta c << 1$.

In old papers the term associated with the velocity spread (to be more exact, the spread over particle momenta ($\Delta p/p$) was left in the expression for the anti-Hermitian part of the plasma permittivity. In the course of the new analysis Kuznetsov and Tsap (2007) conclude that the non-relativistic approximation cannot be used for investigation of the generation of upper-hybrid waves at the double plasma resonance when $s >> 1$. And the authors used the condition of the cyclotron resonance of waves and accelerated electrons in the form:

$$\dot{\psi}_s = \omega - \frac{s\omega_B}{\Gamma} - k_z \upsilon_z = 0 \qquad (5)$$

where $\dot{\psi}_s$ is the time derivative of the phase difference between the waves and the gyrorotating particles, v_z is the longitudinal component of electron velocity (v), and $\Gamma = (1 - v^2/c^2)^{-1/2}$ is the relativistic factor.

Here, it is necessary to recall that Zlotnik *et al.* (2003) assume that the dispersion relation (A.6) is correct only inside the hybrid band. They obtained very narrow maximum of the growth rate due to at the estimation of $\Delta k_\perp/k_\perp$, the velocity dispersion $\Delta v_\perp /v_\perp$ was missed as the infinitesimal quantity. This is already examined in detail in Chernov (2006). Zlotnik *et al.* (2003) assume also that many authors (Winglee and Dulk, 1986; Kuznetsov and Tsap, 2007) erroneously conclude that the kinetic instability of plasma waves described by the dispersion relation (A.6): $\omega^2 \cong \omega_p^2 + \omega_B^2 + 3k_\perp^2\upsilon_T^2$ - may contain several harmonics, while it is valid only inside the interval $\Delta\omega \le \omega_B$. This assertion is correct, mainly, without taking into account relativistic correction and for the strictly perpendicular propagation. Zlotnik and Sher (2009) showed that in this case the harmonics, which adjoin the hybrid band on the top, give the overstated contribution to the value of increment, and this leads to the expansion of its maximum. To answer this question new calculations with the precise dispersion relation will only help. At least, Kuznetsov and Tsap, 2007 assert that comparison with the exact solution of the dispersion relation shows that the equation of upper-hybrid waves (A.6) describes well the behavior of the oscillation branch with normal dispersion even at $\lambda \ge 1$, including the frequencies above the hybrid band. Moreover, Robinson (1988) has shown that weakly relativistic effects (especially in the case of *slightly non-transversal propagation*) cause the branches with normal dispersion corresponding to different harmonics to reconnect to one another at $\omega \approx s\omega_B$. As a result, a single continuous branch is formed. In addition, the condition of touching of the loss-cone boundary and the resonance curve can be satisfied only for one certain value of s. Since the contribution of the term associated with this harmonic will considerably exceed the contribution of other terms in the sum for the loss cone with a sharp boundary (when $\theta_c \to 0$; see the following), we can neglect the summation over harmonics and assume that the growth rate $\gamma \approx \gamma_s$, where γ_s is the growth rate at the s-th harmonic.

In the course of the analysis Kuznetsov and Tsap (2007) derived the final form of the imaginary part of the dielectric permeability (in the relation for γ):

$$\mathrm{Im}\,\varepsilon_{\parallel}^{(s)} \approx -2\pi^2 m^4 c^2 \frac{\omega_p^2}{k^2}\frac{n_b}{n_0}\Gamma^3 J_s^2\left(\frac{k_\perp p_\perp}{m\omega_B}\right)\times$$
$$\left[\frac{\partial\varphi(p)}{\partial p} + \frac{\varphi(p)\tan\theta_c}{p\Delta\theta_c}\left(\frac{s\omega_B}{\Gamma\omega\sin^2\theta_c} - 1\right)\right]\frac{\Delta p_z}{p}\,, \qquad (6)$$

where the momentum $\mathbf{p} = (p_z; p_\perp)$ and the parameter Γ correspond to the point of tangency $p_{\perp 0} = p_{z0}\ tan\ \theta_c$ (see Figure 18), $J_s(\xi)$ is the first-order Bessel function.

The derivation of Formula (6) somewhat differs from the corresponding procedure in the work of Zheleznyakov and Zlotnik (1975) because of another normalization condition for the function $f\mathbf{p}(\mathbf{p})$ and a misprint in the tensor of the

dielectric permeability by the coefficient in front of the matrix (which contains the relativistic electron mass ($\tilde{m}$) rather than the rest one (see Appendix in Kuznetsov and Tsap (2007).

As a result of calculations, for the Maxwellian distribution of particles over momentum ($\varphi_1(p) = A_1 exp(-p^2/2p_h^2)$) of the loss-cone type (4) and real values of the velocity spread (~0.1), the modulation depth between the peaks of the growth rates turns out to be too small. However, calculations performed with a power-law velocity distribution function with an index of power of 8–10 yielded the modulation depth that was quite sufficient for the ZP formation at many harmonics (Figure 19).

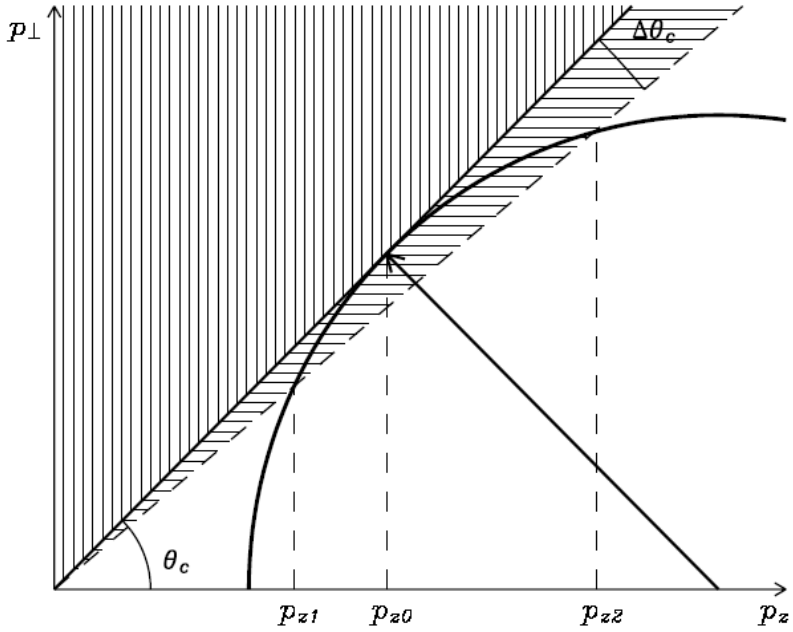

Figure 18 Schematic of the loss-cone distribution and the resonance curve in the space of electron momenta (from Kuznetsov and Tsap, 2007).

A steep power-law spectrum of particles can be considered as an analog of a small velocity dispersion, although such spectra are sometime observed, especially in repeated bursts of hard X-ray emission (data from RHESSI).

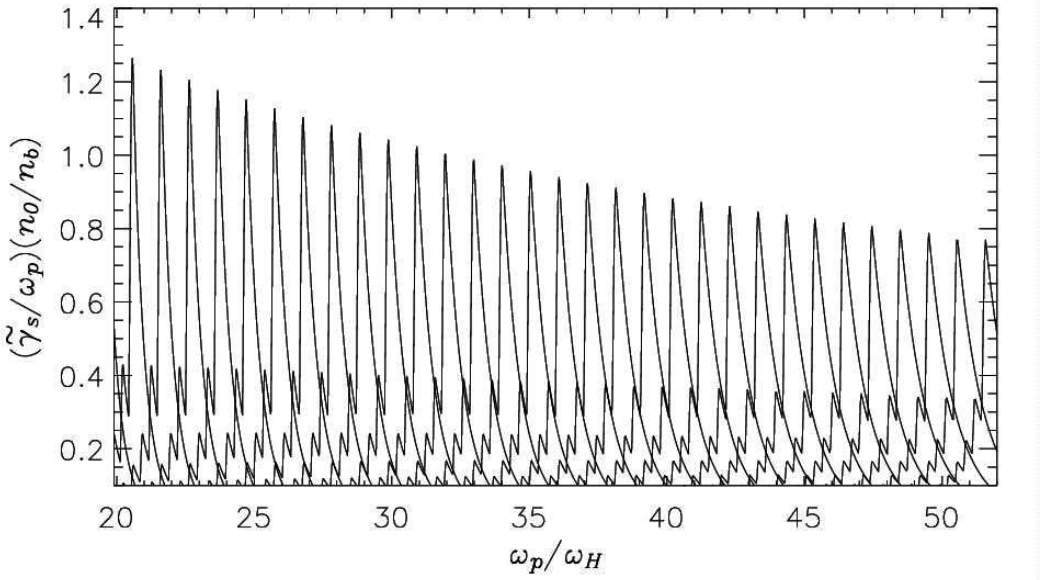

Figure 19 The dependence of the maximal growth rate of upper-hybrid waves on the plasma parameters for the power-law distribution of electrons over momentum (from Kuznetsov and Tsap, 2007).

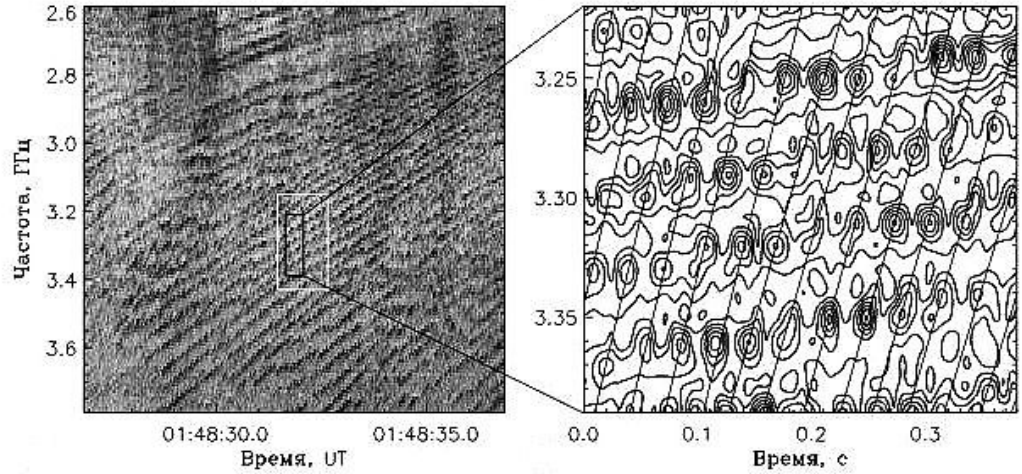

Figure 20 ZP in the frequency range 2.6–3.8 GHz in the event April 21, 2002. The magnified fragment of the spectrum (on the right) demonstrates the superfine structure of stripes in the form of periodic millisecond spikes, which, for better visualization, are shown by contour levels of the intensity (from Kuznetsov, 2007).

Kuznetsov and Tsap (2007) and Kuznetsov (2007) applied their results to interpret 34 ZP stripes with a superfine structure in the form of millisecond spikes in the 2.6–3.8 GHz frequency range (Figure 20) under the assumption that the electron beams were generated strictly periodically. However, if we consider the possibility of simultaneous excitation of waves at 34 DPR levels in the corona, assuming that the plasma density depends on the altitude by the conventional barometric formula $f_P = f_{P0} \exp[-(h - h_{B0})/10^4 T]$ and the magnetic field, by the formula derived in Dulk and McLean (1978) from the radio data, $B = 0.5\ (h/R_s)^{-1.5}$ where R_s = is the Sun radius, then we obtain that 34 DPR

levels extend in the corona up to altitudes of ~65000 km, which, according to current knowledge, correspond to the plasma frequency ~250 MHz.

We calculated the DPR levels shown in Figure 21 by using a barometric formula with the commonly accepted coronal plasma parameters: the electron temperature $T_e = 1.2 \cdot 10^6$ K and the initial plasma frequency $f_{P0} = 3800$ MHz at the altitude $h_{B0} = 20000$ km. If we use a dipole dependence of the magnetic field for cyclotron harmonics, then the DPR resonances at harmonics with $s \geq 50$ will occur at altitudes of higher than 100000 km. Thus, the simultaneous excitation of waves at 34 levels in the corona is impossible for any realistic profile of the plasma density and magnetic field (if do not assume smaller, on the order of magnitude, local density and magnetic field scale heights). For example, if we assume that the magnetic field decreases with altitude more slowly (see, e.g. Figure 55 in Zheleznyakov (1995)), then there will be only a few DPR levels at low harmonics. It should be noted that, as a rule, only several first cyclotron harmonics are easy to excite, whereas the excitation of harmonics with $s > 50$ is hardly possible.

In this connection, let us note that in the following paper (Kuznetsov, 2008) the author proposed alternative mechanism: a model in which the superfine temporal structure is formed due to modulation of the radiation by downward propagating MHD oscillations. The wavelet analysis shown a decrease of the period of spikes (from 40 ms at 2.6 GHz to 25 ms at 3.8 GHz). Variation of the observed period of oscillations is caused by a variation of the speed of the DPR levels (due to the Doppler effect). It was found that in the considered event 21 April 2002 the MHD oscillations should have the period about 160 ms and the speed about 1500 km s^{-1}. This model allows to explain the observed variation of the pulse period with the emission frequency.

However, the superfine stripe structure in the form of millisecond spikes is apparently produced during the generation of the primary continuum radio emission, rather than arises in the course of ZP formation. This is confirmed by the detailed analysis of the time evolution of the spectral amplitudes of continuous radiation several seconds before the appearance of the ZP. It is seen from Figure 22 that, when there is no yet regular ZP stripes, the time dependence of the radiation intensity at the frequency 3.19 GHz clearly exhibits regular spikes with a period of ~30 ms. This period is then present in the ZP (see Figure 20). Thus, the superfine structure is not a consequence of wave excitation at DPR levels.

The superfine structure was also observed in the meter wavelength range. It was shown in Chernov *et al.* (1998) that such a spiky structure can arise due to periodic acceleration of fast particles provided that the simultaneous splitting of the ZP stripes is caused by the excitation of whistlers under the conditions of the normal and anomalous Doppler effects (new beams).

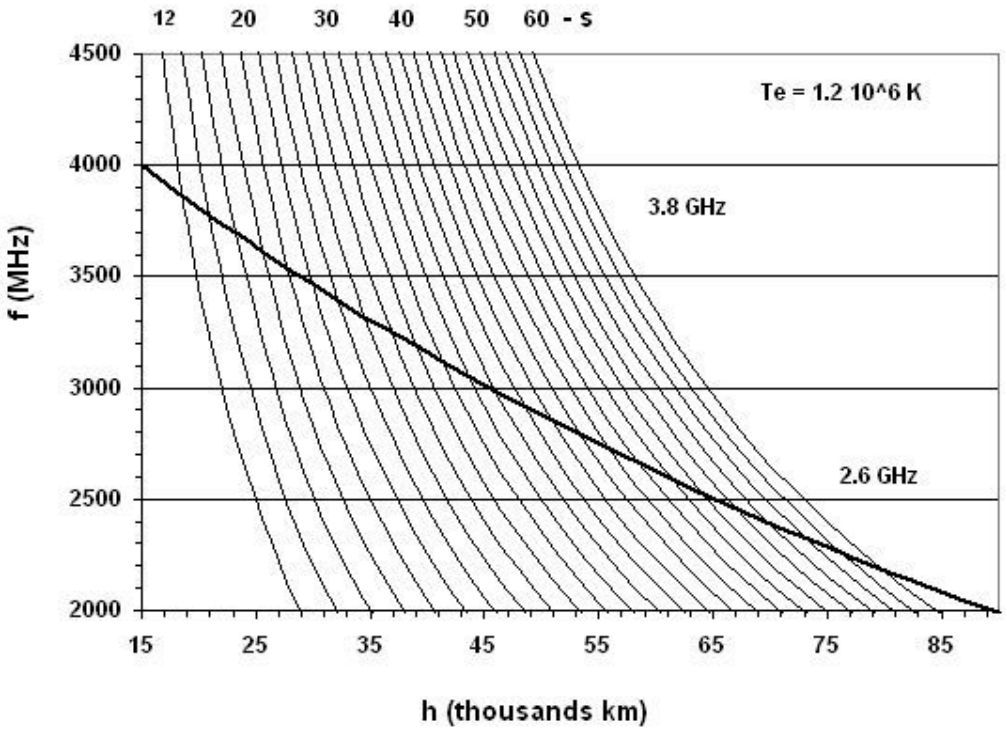

Figure 21 Altitude dependence of the plasma frequency in accordance with the barometric law (heavy line) and altitude profiles of the electron cyclotron harmonics *s* (light lines) in the solar corona. For the electron temperature $T_e = 1.2 \cdot 10^6$ K and initial frequency $f_{P0} = 3800$ MHz at an altitude of $h_{B0} = 20\,000$ km, 34 DPR levels form between 2600 to 3800 MHz plasma layers (from Laptuhov and Chernov, 2009).

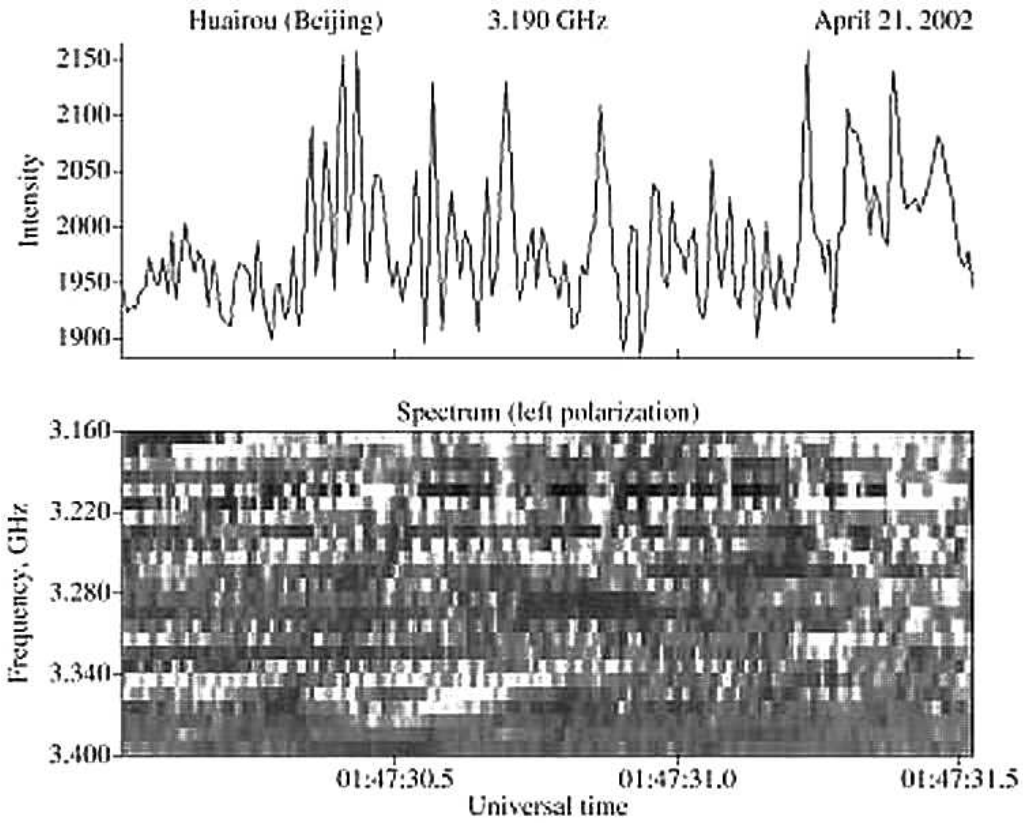

Figure 22 Superfine structure of the continuum in the form of spikes with a period of ~30 ms (from Laptuhov and Chernov, 2009).

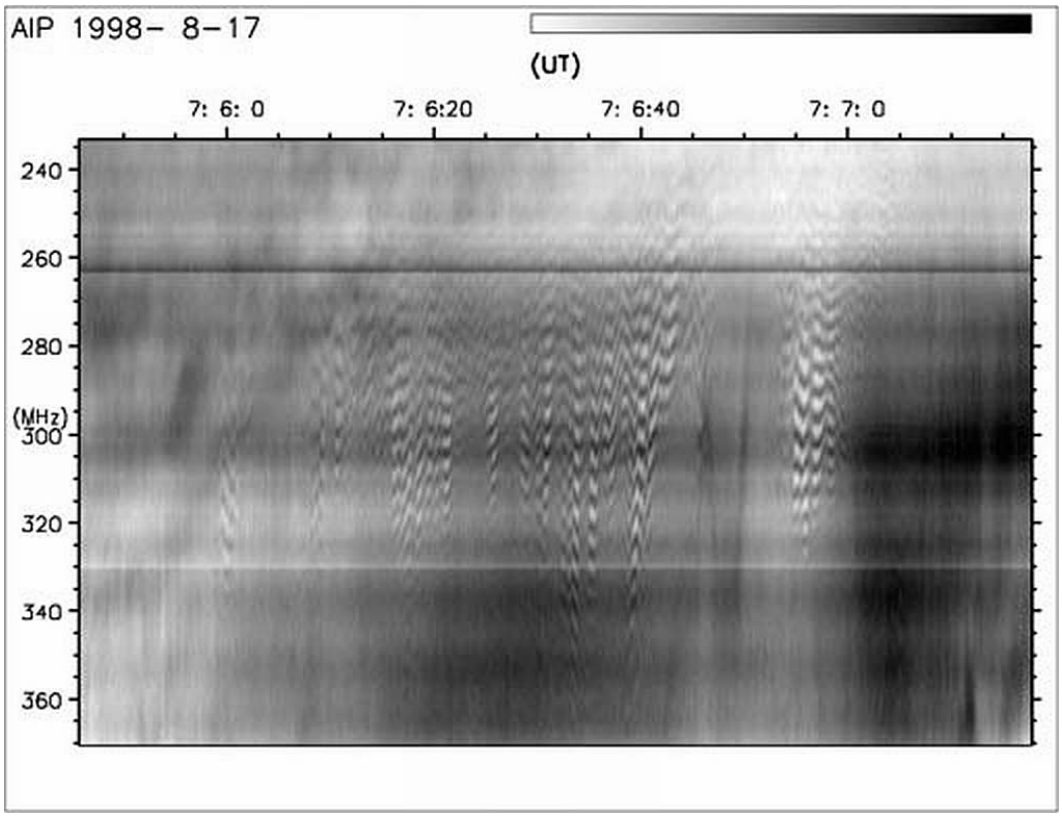

Figure 23 Dynamic radio spectrum with zebra patterns in fast drifting envelopes recorded on 17 August 1998 by the spectrograph of the Astrophysical Institute Potsdam (from Zlotnik et al. 2009).

Zlotnik *et al*. (2009) give an analysis the occurrence of zebra patterns in a fast drifting envelopes of continuum absorption, based on radio spectra of the Astrophysical Institute Potsdam shown in Figure 23. For the explanation of ZP in fast drifting (type III burst-like) envelopes it is proposed to consider complementary multinonequlibrium components of the coronal plasma in the DPR model. ZPs should be related with the emergence of fast particle beams. But prior to the electron beam emergence, the nonequilibrium plasma consists of two components: one having a loss-cone distribution f_1 with velocity υ_1 and causing the background continuum and another one f_2 of DGH type (Dory, Guest, and Harris, 1965) with velocity υ_2 being able to provide the DPR effect and thus causing the ZP.

The loss-cone component is denser and cooler than the DGH component. Thus, for many reasons the stronger continuum can dominate the zebra pattern, making it invisible on the dynamic spectrum. If the electron beam emerges, it fills the loss cone, quenches the loss-cone instability (according to Zaitsev and Stepanov (1975)), and causes a type III-like burst in absorption. The switch-off of the continuum during electron beam passage makes the zebra pattern visible against the absorption burst background. Some specific parameter conditions should be fulfilled:

- for the zebra structure excitation by the DGH component f_2 ($\upsilon_2 / \upsilon_T \sim 15 – 30$) there exist reasonable intervals of velocity $\upsilon_1 \sim (1/6 – 1/2)\ \upsilon_2$ and electron number density $N_2 < N_1 < (10^2 – 10^7)N_2$ for the component f_1 where the proposed generation scheme is valid;

- $N_b >> N_1$ is a necessary condition for the absorption burst;

- the proposed scenario is only valid if the beam velocity ($\upsilon_b \approx c/3$) is much greater than the bulk velocity of electrons at the loss cone ($\upsilon_2/\upsilon_1 \approx 3 - 6$) but the beam does not excite plasma waves.

- the beam electrons with great longitudinal and small transverse velocities fill the loss cone, while the electrons with great transverse and small longitudinal velocities enrich the DGH function f_2 with additional electrons, then an enhanced brightness of zebra stripes is observed.

If even one of these conditions is broken, the ZP can hardly appear. The authors conclude that the described scheme quite naturally explains the (at first glance enigmatic) appearance of a zebra pattern during electron beam passage without a type III burst in emission. However, two distributions (DGH and loss-cone) can exist simultaneously but rather in different places of the radio source.

Besides, it should be assigned several properties of ZP stripes in the spectrum, not noted in Zlotnik *et al*. (2009). Not all the type III-like envelopes have negative frequency drift, it is possible to note almost instantaneous in the broadband (07:06:31 UT) or even with the positive drift (07:06:25 UT). ZP is visible between the envelopes. It is possible to trace continuous ZP stripes lasting through five envelopes with the spasmodically changing drift. ZP is only strengthened during the envelopes and it is experienced the sharp jumps of drift (by zigzags).

Such almost vertical pulsating envelopes of ZP are not so rare phenomena. For instance, let us see an excellent sample in Figures 6C in Slottje (1972). And in the event 3 July 1974 similar ZP envelopes were continuing during several hours (Slottje ,1981; Chernov, 1976). Smooth or abrupt changes in the frequency drift of ZP stripes in the event 25 October 1994 were discussed in Chernov (2005) on the basis of the natural mechanism of the formation of stripes in absorption due to the diffusion of fast particles on whistlers. The whistler waves are always generated simultaneously with the plasma waves at upper hybrid frequency by fast particles with the loss-cone velocity distribution. This diffusion process is examined in Chernov (1990) and in more detail in Chernov (1996; 2005). The important feature was there noted: the changes in the sign of the frequency drift correlate with the change in the direction of the spatial drift of the ZP radio source (see Figure 32 and 64 in Chernov (2006)). The loss-cone distribution function changes due to the diffusion and the whistler generation switches from normal Doppler resonance to anomalous one. In such a case whistler group velocity changes the direction to the opposite, which results the change of the sign of the frequency drift of ZP stripes. Additional particle injection can only accelerate this process and strengthen the instability of whistlers, with which can be related the strengthening of ZP in drifting envelopes in the event examined in Zlotnik *et al*. (2009).

Thus, in the model with the whistlers the absorptive ZP stripes are formed also due to the quenching of the loss-cone instability, but due to only the scattering of fast particles on whistlers and only in the whistler wave packet volume. This mechanism explains the spasmodically changing frequency drift, and it does not require any complementary strict specific parameters.

The appearance of absorptive bursts depends strongly of parameters of new beams. Chen and Yan (2008) shown that the large scale beams with longtime injection (~ 1 s) are responsible for broadband type III- like absorptive bursts, and only the small scale beams with very short injection time (~ 0.2 ms) could be responsible of absorptive spikes (see Figure 7 in Chen and Yan (2008)). New beams with great longitudinal velocities enrich the whistler generation at

anomalous Doppler resonance (Chernov, 1996) and as a consequence, the formation of ZP stripes. This explains strengthening of ZP- stripes during drifting envelopes (Figure 23). We could propose the same effect includes in bright ZP stripes in absorptive type III- like bursts in the event 13 December 2006 (Figure 12). However, in such a case the whistler generation and as a consequence, the formation of ZP stripes depends strongly also of the velocity distribution in the new beams.

In the recent small critical review of Zlotnik (2009) the advantages of DPR model and the main failures of the model with whistlers are refined. The author asserts that the theory based on the DPR effect is the best-developed theory for ZP origin at the meter-decimeter wavelengths at the present time. It explains in a natural way the fundamental ZP feature, namely, the harmonic structure (frequency spacing, numerous stripes, frequency drift, etc.) and gives a good fit for the observed radio spectrum peculiarities with quite reasonable parameters of the radiating electrons and coronal plasma. The statement that the theory based on whistlers is able to explain only a single stripe (e.g., a fiber burst) was made in Zlotnik (2009) without the correct ideas of whistler excitation and propagation in the solar corona.

First of all, Zlotnik uses a wrong term "oscillation period" of whistlers. Actually, the loss-cone particle distribution is formed as a result of several passages of the particles in the magnetic trap. But the whistler amplification length is always small (of $\leqslant 10^8$ cm in comparison with the length of the magnetic trap of $>10^9$ cm) for any energy of fast particles (Breizmann, 1987, Stepanov and Tsap, 1999). According Gladd (1983) the growth rate of whistlers for relativistic energies of fast particles decreases slightly if the full relativistic dispersion is used. In this case, the whistlers are excited by anisotropic electron distributions due to anomalous Doppler cyclotron resonance. Thus, our conclusion, that the entire magnetic trap can be divided into the intermittent layers of whistler amplification and absorption remains valid for a broad energy range of fast particles.

In Zlotnik (2009) the main matter is ignored that the model involving quasilinear interaction of whistlers with fast particles allows one to explain all the fine effects of the ZP dynamics, mainly the superfine structure of ZP stripes and oscillating frequency drift of the stripes synchronously with the spatial drift of radio sources.

4.2. MODELS OF ZP FORMATION DURING RADIO WAVE PROPAGATION IN THE CORONA

Let us consider the capabilities of alternative models. One of the first such models was proposed in Laptuhov, Chernov and Kovalev (2005) and further developed in Laptuhov and Chernov (2006), where a one-dimensional inhomogeneity was considered in which the plasma and field parameters varied periodically in space along one coordinate x with a period $L_x = L$ (e.g., in the presence of nonlinear thermal structures) and the magnetic field $\mathbf{B} = (0, 0, B)$ was perpendicular to the inhomogeneity gradient and directed along the z axis.

The wave equation obtained from Maxwell's equations and hydrodynamic equations for the perturbed velocity of electrons and ions in a cold nonuniform magnetoactive plasma yields a generalized vector equation for the perturbed electric field, which has separate solutions for ordinary and extraordinary waves. The problem is reduced to deriving the corresponding dispersion relations in a

spatially inhomogeneous medium in which the profiles of both the plasma density and magnetic field are approximated by stepwise functions. An analysis of the solutions to this problem revealed the existence of transparent regions separated by opaque regions of different width depending on the inhomogeneity scale L.

Thus, the dark ZP stripes observed in the radio emission spectrum can form due to the existence of opaque regions in a spatially periodic medium. The frequency separation between transparent regions increases with frequency (in agreement with observations). The number of harmonics grows with increasing amplitude of the inhomogeneity, but is independent of the ratio of the plasma frequency to the gyrofrequency in the source. This may help to overcome all the difficulties in explaining the large number of ZP stripes and small values of the magnetic field determined from the frequency separation of stripes (e.g., in the DPR-based model).

Practically at the same time, Barta and Karlicky (2006) analyzed a similar problem in which the formation of harmonics during the propagation of a wave through regular inhomogeneities (such as oscillations behind a shock front) was considered in a simplified approach. The wave equation was written for an unmagnetized plasma, the dispersion relations for harmonics were not derived, and solutions for the amplitudes of reflected and transmitted waves were searched. From the conservation laws and boundary conditions admitting the existence of nontrivial solutions, the frequency dependence of the transmission coefficient was found. As a result, multiple narrow harmonics (transmission regions, called interference stripes) separated by opacity (reflection) regions were obtained. In view of analogy with the results of Laptuhov and Chernnov (2006), it is worth comparing the parameters of transmission regions obtained in these two papers.

In Ledenev, Yan and Fu (2006), a similar problem was considered in an even simpler approach in which the interference pattern produced by the incident rays and those reflected from regular inhomogeneities was analyzed. The problem was solved in the geometrical optics approximation by using the eikonal equation (by analogy with the problem of light propagation through a crystal lattice). The size of the radio emission source was assumed to be infinitely small, and the emission spectrum was considered to be sufficiently broad. Evidently, in case of radio wave reflection from smooth inhomogeneities, the interference pattern cannot be as contrast as that produced by light reflected from a solid body. Moreover, the ordinary and extraordinary waves are reflected from layers with different plasma densities. Therefore, the modulation depth of the total interference pattern produced by many small-size sources is relatively small.

4.3. PROPAGATION OF RADIO WAVES THROUGH *N* IDENTICAL INHOMOGENEOUS LAYERS

In Laptuhov and Chernov (2006), the propagation of electromagnetic waves through a spatially periodic plasma was investigated to explain the ZPs observed in solar radio bursts. The possibility of existence of one-dimensional spatially periodic structures in the solar atmosphere was demonstrated in Kovalev (1990); Laptuhov (1991). Laptuhov and Chernov (2006) assumed that the waves propagate in a unbounded collisionless plasma along the x axis perpendicular to the magnetic field $\mathbf{B} = (0, 0, B(x))$. Here, we will consider a more realistic model in which a spatially periodic plasma occupies a region of thickness NL containing N identical plasma layers of thickness L. For simplicity, each layer is assumed to

consist of two piecewise-homogeneous layers with the thicknesses $a < L$ and $b = L - a$. In the regions $x < 0$ and $x > NL$, the plasma is uniform.

Let us consider the propagation of broadband radio emission in such a plasma. As a matter of fact, the region occupied by the spatially periodic plasma is a frequency filter with multiple transparency windows separated by opaque regions (see Figure 1 in Laptuhov and Chernov (2006)). If a broadband radiation is incident at the filter input ($x = 0$), then, at the output ($x = NL$), the radiation spectrum will contain only the frequencies that correspond to the transparency windows of the filter, while the amplitudes of waves with frequencies corresponding to opaque regions will be practically zero. As a result, after passing through such a filter, a structure similar to the ZP observed in the solar radio spectrum will form. This is the essence of the physical mechanism that was proposed in Laptuhov and Chernov (2006) to explain the ZP formation in solar radio emission. In this case, the mechanism for the generation of primary broadband radio emission can be arbitrary (e.g., beam – plasma or cyclotron loss-cone instability (Zheleznyakov, 1995). An analysis of these mechanisms goes beyond the scope of the present study.

Let us first analyze the propagation of an ordinary wave, the field of which is described by the following simple formula (see Eq. (8) in Laptuhov and Chernov (2006)):

$$\frac{d^2E}{dx^2} + k^2E = 0, \quad k^2 = \frac{\omega^2 - \omega_p^2}{c^2}, \quad \omega_p^2 \equiv \omega_e^2 + \omega_i^2 \tag{7}$$

The plasma frequency $\omega_p(x)$ and the corresponding constants k_m in different plasma regions are defined by the formulas

$$\begin{aligned}
&\omega_p(-\infty < x < 0) = \omega_0, \quad \omega_p(NL < x < \infty) = \omega_3, \\
&\omega_p((n-1)L < x < a + (n-1)L) = \omega_1, \quad n = 1,2...N, \\
&\omega_p(a + (n-1)L < x < nL) = \omega_2, \quad \omega_0 \geq \omega_3 \geq \omega_1, \\
&k_m \equiv \sqrt{(\omega^2 - \omega_m^2)}/c, \quad m = 0,1,2,3.
\end{aligned} \tag{8}$$

where all of the four frequencies ω_j, ($j = 0,1,2,3$) are constant. In this case it is assumed that in the regions $x < 0$ and $x > NL$ the plasma is uniform, and between them ($0 < x < NL$) it is located N of the identical layers, each of which is piecewise-uniform and has a thickness L. Let an electromagnetic wave with the frequency $\omega > \omega_0$ propagates along the x axis in the region $x < 0$. Then, taking into account wave reflection from the region $0 < x < NL$, a general solution to Eq. (7) in the region $x < 0$ can be written as

$$E(x < 0) = E_0 \exp(ik_0x) + E_r \exp(-ik_0x), \tag{9}$$

where E_0 is the amplitude of the incident wave, which is assumed to be given, and E_r is the amplitude of the reflected wave.

Let us now write the solution to Eq. (7) in the region $0 \leq x \leq NL$. We introduce the notation

$$Y_{1n} \equiv E(x = nL), \quad Y_{2n} \equiv \frac{dE(x = nL)}{dx}, \; n = 0,1,...N. \tag{10}$$

If the constants Y_{10} and Y_{20} are known, then, using Eqs. (12) – (14) from Laptuhov and Chernov (2006), we find

$$Y_{i1} = M_{ij} Y_{j0}, \quad i = 1,2, \quad j = 1,2. \tag{11}$$

Hereinafter, we perform summation over repeating indices from j = 1 to 2. The components of the matrix M for the case $\omega_1 \le \omega_0 \le \omega \le \omega_2$ are as follows:

$$\begin{aligned} M_{11} &= \cos(g)ch(f) - k_1 \sin(g)sh(f)/q_2, \\ M_{12} &= \sin(g)ch(f)/k_1 + \cos(g)sh(f)/q_2, \\ M_{21} &= q_2 \cos(g)sh(f) - k_1 \sin(g)ch(f), \\ M_{22} &= \cos(g)ch(f) + q_2 \sin(g)sh(f)/k_1, \\ g &\equiv k_1 x_1, \quad f \equiv q_2(L - x_1), \quad q_2 \equiv \left(\omega_2^2 - \omega^2\right)^{1/2}/c. \end{aligned} \tag{12}$$

For the case of $\omega_1 \le \omega_0 \le \omega_2 \le \omega$ the components of the matrix M have the form:

$$\begin{aligned} M_{11} &= \cos(g)\cos(f) - k_1 \sin(g)\sin(f)/k_2, \\ M_{12} &= \sin(g)\cos(f)/k_1 + \cos(g)\sin(f)/k_2, \\ M_{21} &= -k_2 \cos(g)\sin(f) - k_1 \sin(g)\cos(f), \\ M_{22} &= \cos(g)\cos(f) - k_2 \sin(g)\sin(f)/k_1, \\ f &\equiv k_2(L - x_1), \quad k_2 \equiv \left(\omega^2 - \omega_2^2\right)^{1/2}/c. \end{aligned} \tag{13}$$

Note that the eigenvalues ξ of the matrix M, which are defined by the equation

$$\det(M_{ik} - \xi\delta_{ik}) = \xi^2 - 2p\xi + 1 = 0, \quad 2p = M_{11} + M_{22} \tag{14}$$

coincide with the parameter ξ in formula (16) from Laptuhov and Chernov (2006) and p is defined by the same formula. In addition, it should be kept in mind that $det(M_{ik})$=1.

Since all N layers are identical, it follows from formula (11) that

$$\begin{aligned} &Y_{in} = M_{ij}^n Y_{j0}, \quad M_{ij}^1 \equiv M_{ij}, \quad n = 1,2,...N, \\ &M_{ij}^n = M_{ik} M_{kj}^{n-1}, \quad M_{kj}^0 = \delta_{kj}, \quad i,j,k = 1,2. \end{aligned} \tag{15}$$

where δ_{kj} is the Kronecker delta.

In the region $x > NL$, there is only the transmitted wave. Therefore, in this region, we have

$$\begin{aligned} &E(x \ge NL) = E_t \exp(ik_3(x - NL)), \\ &E_t \equiv Y_{1N}, \quad Y_{2N} = ik_3 Y_{1N}. \end{aligned} \tag{16}$$

Calculating Y_{2N} / Y_{1N} with allowance for formulas (15) and (16) yields the first equation for the unknown constants Y_{10} и Y_{20}. The second equation for these constants can be obtained from Eqs. (9) – (10) if we take into account that the field $E(x)$ and its derivative dE/dx are continuous at the point x = 0. Solving the resulting set of two linear equations, we express Y_{10} and Y_{20} and, thus, all the coefficients Y_{in} (see Eqs. (15)) through E_0 and the parameters of the medium. After simple manipulations, we obtain

$$\frac{E_r}{E_0} = \frac{M_{22}^N - k_3 M_{11}^N / k_0 - i\left(M_{21}^N / k_0 + k_3 M_{12}^N\right)}{M_{22}^N + k_3 M_{11}^N / k_0 + i\left(M_{21}^N / k_0 - k_3 M_{12}^N\right)},$$

$$\frac{E_t}{E_0} = \frac{2}{M_{22}^N + k_3 M_{11}^N / k_0 + i\left(M_{21}^N / k_0 - k_3 M_{12}^N\right)}, \qquad (17)$$

$$K_t \equiv \mathrm{mod}\left(\frac{k_3 E_t^2}{k_0 E_0^2}\right), \quad K_r = \mathrm{mod}\left(\frac{E_r^2}{E_0^2}\right) = 1 - K_t,$$

where K_t is the transmission coefficient of the system of plasma layers with the total thickness NL. By definition, this coefficient is equal to the ratio of the intensity $\mathbf{Q} = c[\mathbf{E},\mathbf{B}]/4\pi$ of the transmitted wave to that of the incident wave. It can easily be shown that the coefficient of reflection from N inhomogeneous plasma layers is $K_r = 1 - K_t$.

Note that the results obtained can also be generalized to the case of extraordinary waves described by Eq. (17) in Laptuhov and Chernov (2006) (cf. Eq. (7)). Below, we will consider some examples of calculating the reflection and transmission coefficients for different parameters of plasma inhomogeneities.

The number of stripes and their shape depend on the parameters (such as the size and number) of inhomogeneities. The profile of the harmonics of the reflection coefficient in the form of narrow peaks separated by a relatively wide frequency intervals (see Figure 23) can be interpreted as radiation stripes similar to those present in the lower spectrum in Figure 16 in Chernov (2006). Thus, in this case, the ZP is probably observed in reflected radiation. Note that the harmonics of the reflection coefficient in Figure 23 agree better with observations than the results of similar calculations in Barta and Karlicky (2006) presented in Figure 24. In our case, this is an even comb of harmonics in which the frequency separation between neighboring harmonics increases gradually with frequency, whereas in Barta and Karlicky (2006), intense harmonics alternate with weak ones. Presumably, inhomogeneities in the form of density dips, which were considered in Barta and Karlicky (2006), cannot provide the observed widths of the ZP stripes. Moreover, we take into account the magnetic field and harmonics of an ordinary wave agree better with observations.

For a smaller number of larger inhomogeneities with a = 45 m, the frequency profile of the transmission coefficient (see Figure 25) yields nearly symmetric harmonics, which are most frequently observed (see the upper spectrum in Figure 16 in Chernov (2006)).

Figure 26 shows the results of calculations of the transmission coefficient in the microwave range. It is seen that, after passing through inhomogeneities with a thickness of L = 3 m, the spectrum of ordinary waves consists of symmetric harmonics, the frequency separation between which increases gradually with frequency, which agrees with observations. The sufficiently large number of harmonics are produced when the number of inhomogeneities is >10.

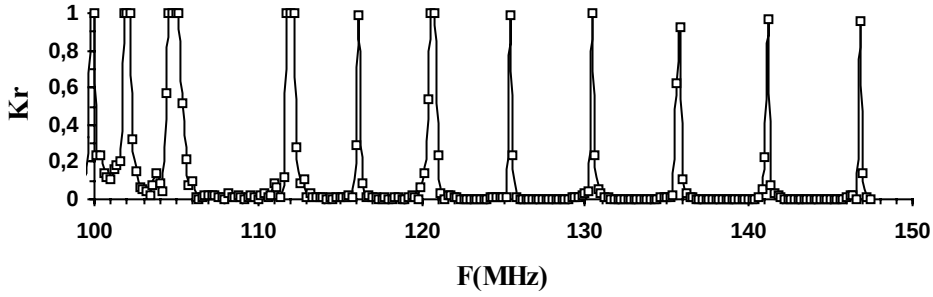

Figure 23 The reflection coefficient K_r of ordinary waves as a function of the frequency F for $n_1 = n_2 \cdot 0.84 = n_3$, $n_0 = n_2$, $a = b = 10$ m, $n_2 = 1.2d + 8$, and $N = 50$ (from Laptuhov and Chernov, 2006).

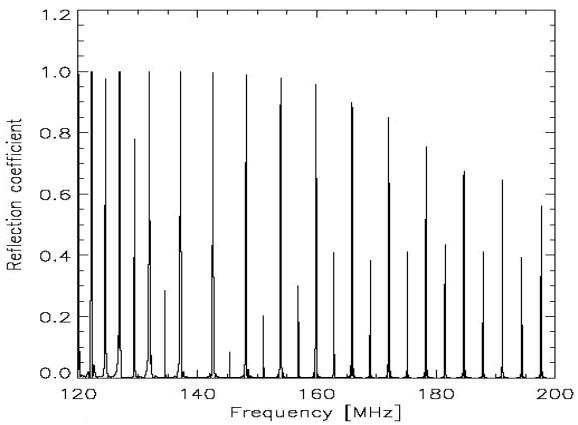

Figure 24 The reflection coefficient $R = 1 - T$ for the series of 50 density wells finished by the density drop as a function of the frequency of an incident wave (from Barta and Karlicky, 2006).

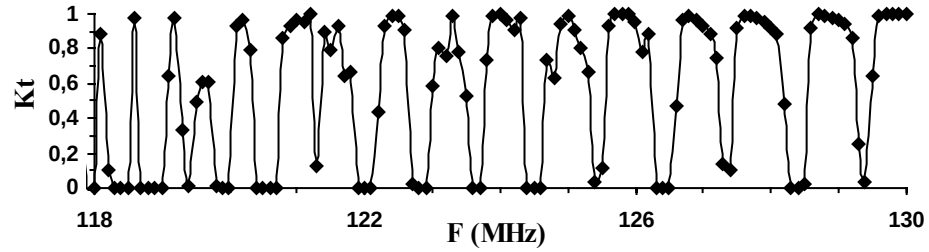

Figure 25 The transmission coefficient K_t of ordinary waves as a function of the frequency F for $n_0 = n_3 = 1d + 8$, $n_2 = 1.5n_0$, $n_1 = n_2/2$, $a = 45$ m, $b = a$, $N = 10$, and $B = 5$ G (from Laptuhov and Chernov, 2006).

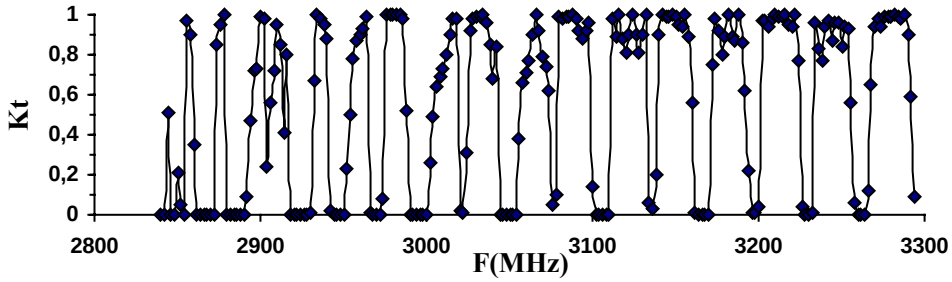

Figure 26 The transmission coefficient K_t of ordinary waves as a function of the frequency F for $n_1 = n_2/\alpha$, $n_0 = 2n_2/(1 + \alpha) = n_3$, $b = L/(1 + \alpha)$, $a = \alpha b$, $L = 3$ m, $\alpha = 2$, $n_2 = 1.0d + 11$, and $B = 100$ G (from Laptuhov and Chernov, 2006).

Some concluding remarks

An analysis of the difficulties arising in different models shows that the improvement of these models necessitates imposing new stringent conditions on the parameters of plasma and waves in the source. The simplest model is related to the propagation of radio waves through regular inhomogeneities, because inhomogeneities are always present in the solar corona. In this case, the dynamics of ZP stripes (variations in the frequency drift, stripe breaks, etc.) may be associated with the propagation of inhomogeneities, their evolution, and their disappearance.

The observed frequency difference between neighboring ZP stripes increases with frequency. This corresponds to the propagation of ordinary waves, the electric field of which is parallel to the unperturbed magnetic field, through a spatially periodic plasma. The number of discrete harmonics does not depend on the ratio of the plasma frequency to the gyrofrequency in the source. The latter circumstance can eliminate all the difficulties that arise in explaining the large number of ZP stripes and the small magnetic field value determined from the frequency separation of stripes (e.g., in the DPR based model).

The superfine structure observed in the microwave range, when all the continuous emission consists of spikes (Figure 20), indicates the presence of plasma wave – whistler interaction in the pulsed regime of whistler interaction with ion acoustic waves in the radio emission source generating ordinary waves (this mechanism was considered in Chernov, Yan, and Fu, (2003)). An alternative source of pulsed radio emission may be associated with plasma density pulsations caused by the propagation of a finite amplitude wave. The generation of electron cyclotron maser radiation, which is considered a possible cause of the observed spikes Fleishmann and Mel'nikov (1998), is dominated by extraordinary waves.

4.4. OTHER RECENT MODELS

4.4.1. Nonlinear periodic space – charge waves in plasma

Kovalev (2009) have investigated periodic nonlinear waves that can arise in plasma due to the excitation of potential oscillations by accelerated electrons with unstable distributions. As was noted in Kovalev and Petviashvili (1994), one-dimensional single-peak distributions of accelerated electrons are most likely to exist in the solar flare plasma. Such electron distributions excite resonance Langmuir oscillations with frequencies $\omega_2 < \min\{\omega_B, \omega_P\}$, due to the anomalous Doppler resonance. Low- and high- frequency modes of Langmuir oscillations can form large-amplitude periodic nonlinear waves. The corresponding spectrum of electromagnetic waves excited resonantly by the current of a potential wave is calculated. It is shown that an equidistant spectrum of electromagnetic radiation in plasma can form in the presence of a periodic potential wave.

Thus, the radio emission harmonics can be generated directly in the source in the form of a nonlinear periodic space charge wave in plasma. In Kovalev (2009), a solution in the form of such a wave propagating in a magnetic field was obtained in the hydrodynamic approach (without taking into account wave dispersion). The spectrum near the breaking point, in the vicinity of which the number of harmonics increases substantially, was calculated. Due to electron

bunching, the periodic wave with the spatial period $l = 2\pi u/\omega_2$ has the form of spatially alternating negatively and positively charged layers with an increased and a decreased electron density. In the presence of a wave electric field, the accelerated particles are subject to additional periodic acceleration and deceleration, due to which an electromagnetic wave is generated.

For a sufficiently large amplitude of density oscillations (a), a large number of harmonics with the frequency separation close the electron-cyclotron frequency can be excited. The number of these harmonics is determined by the parameter $N = \frac{3}{2^{3/2}(1-a)^{3/2}}$, characterizing the degree of nonlinearity. Thus, for $a \sim 0.9$, we have $N \approx 34$. Since the radio emission can be generated in a relatively small-size source, the key difficulty of the DPR-based model, namely, the excitation of a large number of harmonics in a distributed source, is overcome (Figure 20). The number of harmonics can be fairly large when one of the plasma oscillation modes is dominating. In this case, the amplitudes of harmonics decrease fairly slowly ($\propto s^{-1/3}$) with increasing harmonic number s.

Due to inverse processes, the energy of background electromagnetic waves can transform into the energy of potential oscillations at the resonance frequencies $s\omega_2$. This can lead to the formation of an absorption zebra pattern consisting of stripes with a depressed radiation intensity.

The efficiency of the quite natural mechanism associated with nonlinear space charge waves depends on whether strong nonlinearity is reached; however, conditions for achieving the nonlinear regime were not considered in Kovalev (2009). The nonlinearity should rapidly increase and disappear in the course of wavebreaking (at $a = 1$).

4.4.2. The new alternative mechanism of the ZP due to development of explosive instability in the system beam – plasma

Observations of ZP during the powerful flares make possible to assume that the particle acceleration to the relativistic velocities and excitation of different wave modes occurs in the radio source. Therefore, probably, it should be take into account other possible interactions of waves and particles. For example, into Fomichev and Fainshtein (1981) was proposed the decay instability of whistlers to the harmonics of the ion sound, which have weak spatial dispersion and small damping at frequencies much less than the ion Langmuir frequency ω_{oi}. In Fomichev, Fainshtein and Chernov (2009) an alternative mechanism of ZP is discussed, due to the development of explosive instability in the system weakly–relativistic beam – nonisothermic plasma. The explosive instability appears in the nonequilibrium system, where there are waves of negative energy (Kadomtsev, Mihailovsky and Tomofeev, 1964), moreover in the resonance triplet negative energy must possess the wave of the highest frequency of ω_3, and two lowest waves ($\omega_{1,2}$) have positive energy. Fomichev, Fainshtein and Chernov (2009) shown, that the mechanism of the generation of the ion-acoustic “saw” as a result of the development of explosive instability in the system the weakly-relativistic flow of protons – strongly nonisothermic plasma is more effective in the energy sense.

The number of harmonics of ionic sound n is determined by two factors: 1) the dispersion of ion sound must be sufficiently small [1]); 2) $\nu_{ef} << \omega$ (ω – the angular frequency of sound), i.e., the n- harmonic of sound must weakly attenuate.

The quasi-hydrodynamic approximation was utilized for describing interaction of the particles of the beam and plasma (Fainshtein and Chernova, 1996; Ginzburg, 1967). Linearizing the hydrodynamic equations for the processes of ~ $exp(i\omega t–ikx)$, a dispersion equation for the system the flow–plasma was obtained:

$$1-\frac{\omega_{0\mathrm{i}}^2}{\omega}-\frac{\omega_{0\mathrm{i}}^2}{c_{\mathrm{s}}^2 k^2}-\frac{\omega_{0\mathrm{s}}^2}{(\omega-kV_0)^2\left(1-\frac{\omega-ck}{3ck}\right)}=0, \tag{18}$$

where $\omega_{0\mathrm{s}}^2 = 4\pi e^2 N_{0s} M_0^{-1}$, $\omega_{0i}^2 = 4\pi e^2 N_0 M^{-1}$; $\omega -$ cyclic frequency, k – wave number; e, M_o, M – electron charge, the rest mass of ion beam, the mass of the ion of the plasma; $\overline{\rho}_s = N_{0s} + \rho_s$; $\overline{V}_s = V_0 + V_s$; ρ_s, V_s, ρ_i, V_i – the deviation respectively of ion concentrations of beam, speed of the ions of beam, concentration of the ions of plasma, velocity of the ions of plasma from their equilibrium values N_{0s}, V_0, N_0, 0. With $V_0/c_s >> 1$, $N_{0s}/N_0 << 1$ from (18) the approximate dispersion equations were obtained:

$$\omega_1 \equiv \Omega \approx c_s k_1 \equiv c_s m q; \tag{19}$$

$$\omega_{3,2} - k_{3,2} V_0 \approx \mp \omega_{0s} + \delta; \frac{\delta}{\omega_{0s}} << 1. \tag{20}$$

Equation (19) describes the ion-acoustic wave (energy positive), and (20) - slow (ω_3, negative energy) and rapid (ω_2, positive energy) beam waves. The number m > 0- is selected from the escape condition of radio emission from the corona. It is easy to determine, that for the slow beam wave (ω_3, k_3), the fast beam wave (ω_2, k_2) and the sound (Ω, q) the conditions of synchronism are satisfied (Tsytovich, 1970). From the conditions of synchronism taking into account (19), (20) we will obtain:

$$mq \approx 2\omega_{0s} V_0^{-1} \tag{21}$$

Since the sound has weak dispersion, the cascade process is possible:

$$mq + mq \to 2mq + mq \to 3mq + mq \ldots mnq.$$

Then, after decomposing nonlinear terms in (1) up to the quadratic terms and after using standard procedure in the weak turbulence (Weiland and Wilhelmsson, 1977; Tsytovich, 1970), the shortened equations for the complex amplitudes of coupling modes are obtained: beam modes $a_j \left(j = 1, 2\right)$ and ion sound $b_k \left(k = 1, 2, \ldots mn\right)$. The analysis of interaction coefficients showed that the systems of such equations describe the stabilized "explosion" (Fainshtein, 1976).

It is shown also, that the increment of the growth of ion sound in this case exceeds considerably the values, obtained in Fomichev and Fainshtein (1981). Therefore the mechanism in question occurs much more effective.

---

[1]) $n^2 q^2 c_s^2 \ll \omega^2_{oi}$; q – wave number of the base ion-sound mode; c_s – ion-sound speed ($c_s^2 = \text{æ} T_e M^{-1}$), M – ion mass , æ – Boltzmann constant.

The generable sound is scattered on the fast protons, which move with a speed of $V \sim V_0 \sim 10^{10}$ cm s^{-1} and according to the mechanism, described in Fomichev and Faishtein (1981), the radiated from the source frequency of $\omega^t \approx mqnV$, and frequency separation between the stripes $\delta\omega^t = mqV$. Taking into account the equation (21) and selected parameters ($N_0 \sim 5 \cdot 10^9$ cm^{-3}, $N_s \cdot N_0^{-1} \sim 10^{-3}$, the constant magnetic field ~ 30 G) we obtain for the emission frequency of ≥ 634 MHz the value of coefficient m = 15, ($7 \cdot 10^2 \leq mn << 15 \cdot 10^3$) and the frequency separation between the adjacent stripes $\delta\omega t \approx 15$ MHz. The obtained value of $\delta\omega^t$ corresponds to the observed frequency separation in the decimeter wave band (Chernov, 2006). In the given above estimations the wavelength of the ion sound ~ 100 m, the initial frequency ~1.0 kHz and the cyclic frequency of the slow beam wave $\omega_3 \sim 7 \cdot 10^2 \, \omega_{0i}$ (that correspond to ~ 10 GHz).

Discrete emission bands are possible when the width of each emission band will be less than the value of frequency separation. This condition imposes restriction on the dispersion of the beam velocities. As show such estimations, executed in Fomichev and Fainshtein (1981), the beam of protons must be sufficiently quasi-monoenergetic, in the case in question $\Delta V_0 / V_0 < 10^{-3}$.

5. Conclusions

We have considered several of the most recent events with new peculiar elements of zebra patterns. All new properties are considered in light both known earlier, and new theoretical models.

In two events (24 July 2004 and 3 November 2004) the large-scale ZP was consisted of small-scale fiber bursts. The appearance of such an uncommon fine structure is connected with the following special features of the plasma wave excitation in the radio source: both whistler and plasma wave instabilities are too weak at the very beginning of the events (the continuum was absent), and the fine structure is almost invisible. Then, whistlers generated directly at DPR levels "highlight" the radio emission only from these levels due to their interaction with plasma waves.

A unique fine structure was observed in the event 13 December 2006: spikes in absorption formed darks ZP stripes against the absorptive type III-like bursts. The spikes in absorption can appear in accordance with well known mechanism of absorptive bursts. The additional injection of fast particles filled the loss-cone (breaking the loss-cone distribution), and the generation of continuum was quenched at these moments, which was evinced by the formation of bursts in absorption. The maximum absorptive effect realizes at the DPR levels. The parameters of millisecond spikes are determined by small dimensions of the particle beams and local scale heights in the radio source.

Thus, in each new event the new special features of the fine structure are revealed. However, they are usually related with the varied conditions in the source. In such a case, one ought not to find the special emission mechanism for each event, which was repeatedly done before.

The DPR model helped to understand several aspects of unusual elements of ZP. In this connection, the calculations of growth rates of upper hybrid waves with different distribution function of fast electrons inside of the loss-cone is very important (Kuzneysov and Tsap, 2007). However, discussions concerning the

validity of taking into account of one or several harmonics in hybrid band continue. In the same time, Laptuhov and Chernov (2009) shown that the simultaneous existence of several tens of the DPD levels in the corona is impossible for any realistic profile of the plasma density and magnetic field (if do not assume smaller, on the order of magnitude, local density and magnetic field scale heights).

Since any known model does not avoid of deficiencies, the attempts to create new theories continue. We examined three new theories.

The formation of transparency and opacity bands during the propagation of radio waves through regular coronal inhomogeneities is the most natural and promising mechanism. It explains all main parameters of regular ZP. The dynamics of ZP stripes (variations in the frequency drift, stripe breaks, etc.) can be associated with the propagation of inhomogeneities, their evolution, and disappearance. Inhomogeneities are always present in the solar corona, however straight evidences of existence in the corona of inhomogeneities with the scales in several meters are absent. Although ion-sound waves could serve as the same.

The model of nonlinear periodic space – charge waves in plasma (Kovalev, 2009) is also very natural mechanism in the solar flare plasma. However, in the case of the intrinsic plasma emission it gives constant frequency separation between stripes of $\approx \omega_B$, while the observations testify the increase of the frequency separation with frequency. Besides, the condition of achievement of the strong nonlinearity remains uncertain.

The mechanism of scattering of fast protons on ion-sound harmonics in explosive instability looks as very uncommon, that requires a number of strict conditions. Although the fast protons are always exist in large flares, and the presence of nonisothermic plasma is completely feasible in the shock wave fronts.

Two last models could be rather realized in large radio bursts. And all three models are related with a compact radio source. The number of discrete harmonics does not depend on the ratio of the plasma frequency to the gyrofrequency in the source in all three models. The latter circumstance can eliminate all the difficulties that arise in the DPR model.

Acknowledgements

We are grateful to Nobeyama, TRACE, RHESSI and SOHO (LASCO/EIT) teams for operating the instruments and performing the basic data reduction, and especially, for the open data policy. G.P.Chernov appreciates the support of the Chinese Academy of Sciences and NSF of China, Prof. Yan Yihua which enabled work with NAOC colleagues, and the Russian Foundation of Basic Research (RFBR), grant Nos. 08-02-00270 and 06-02-39007.

References

Abada-Simon, M., Lecacheux, A., Louran, P., Dulk, G.A., Belkora, L., Bookbinder J.A., Rosolen, C.: 1995, Proceeding of IAU Coll. 151, *Flares and Flashes*, Monograph, Eds. J.Grenier *et al.* v. **454**, p. 32-35.
Aschwanden, M.J.: 2004, *Physics of the Solar Corona*, Pruxis Publishing.
Bárta, M. and Karlický, M.: 2001, *Astron. Astrophys.* **379**, 1045.
Bárta, M. and Karlický, M.: 2006, *Astron. Astrophys.* **450**, 359.
Benz, A.O., and Kuijpers, J.: 1976, *Solar Phys.* **46**, 275.
Chen, B., Yan, Y.: 2008, *Astrophys J.* **689**, 1412.
Chernov, G.P.: 1976a, *Sov. Astron.* **20**, 582.
Chernov, G.P.: 1976b, *Sov. Astron.* **20**, 449.
Chernov, G.P.: 1990, *Sol. Phys*. **130**, 75.

Chernov, G.P.: 1996, *Astron. Reports* **40**, 561
Chernov, G.P.: 1997, *Astron. Lett* **23**, 827.
Chernov, G.P.: 2005, *Plasma Phys. Rep.* **31**, 314.
Chernov, G.P.: 2006, *Space Sci. Rev.* **127**, 195.
Chernov, G. P., Markeev, A. K., Poquerusse, M., Bougeret, J.L., et al.: 1998, *Astron. Astrophys*. **334**, 314.
Chernov, G.P., Yan, Y.H., and Fu, Q.J. : 2003, *Astron. Astrophys*. **406**, 1071.
Chernov, G.P., Yan, Y.H., Fu, Q.J., and Tan, Ch.M.: 2005, *Astron. Astrophys*. **437**, 1047.
Chernov, G.P., Yan, Y.H., Fu, Q.J., Tan, Ch.M. and Wang Sh.J.: 2008, *Solar Phys.* **250**, 115.
Chernov, G.P., Yan, Y.H., Tan, Ch.M., Chen, B. and Fu, Q.J.: 2009. *Solar Phys.* (accepted).
Dabrowski, B.P., P. Rudawy, R. Falewicz, M. Siarkowski, and A. J. Kus,: 2005, *Astron. Astrophys.* **434,** 1139.
Dory, R., Guest, G., and Harris, E.: 1965, *Phys. Rev. Lett.* **14**, 131.
Fainstein, S.M.: 1976, *JETF,* **71**, 1021.
Fainstein, S.M. and Chernova, E.A.: 1996, **109**, 821.
Fleishman, G.D., Stepanov, A.V., Yurovsky, Yu. F.: 1994, *Solar Phys.* **153**, 403.
Fleishman, G. D.and Mel'nikov, V. F.: 1998, *Usp. Fiz. Nauk* **168**, 1265 [*Phys. Usp*. **41**, 1157].
Fomichev V. V. and Fainshtein S. M.: 1981*, Solar Phys*. **71**, 385.
Fomichev, V.V., Fainshtein, S.M. and Chernov, G.P.: 2009, *Plasma Phys. Rep.* **35**, 1032.
Fu, Q.J., Ji, H.R., Qin, Z.H., Xu, Z.C., Xia, Z.G., Wu, H.A. *et al*.: 2004, *Solar Phys.* **222,** 167.
Ginzburg, V.L.: 1967, *Propagation of Electromagnetic Waves in Plasma*, Moscow, Nauka.
Ginzburg, V.L. and Rukhadze, A. A.: 1975, *Waves in Magnetoactive Plasma* (Nauka, Moscow,) [in Russian].
Gladd, N.T.: 1983, *Phys. Fluids*, **26**, 974.
Guo, Y., Ding, M.D., Wiegelmann, T., Li, H.: 2008, *Astrophys. J.* **679**, 1629.
Kadomtsev, B.B., Mihailovsky, A.B. and Timifeev, A.V.: 1964, *JETF* , **7**, 1266.
Karlicky, M. and Barta, M.: 2007, *Adv. Space Res.,* **39**, 1415.
Karlicky, M., Barta, M., Jiricka, K. et al.: 2001, *Astron. Astrophys.* **375**, 638.
Klassen, A.: 1996*, Sol. Phys*. **167**, 449.
Kovalev, V. A.: 1990, *Kinemat. Fiz. Nebesn. Tel* **6**, 38.
Kovalev, V. A.: 2009, *Plasma Phys. Rep.* **35**, 394.
Kovalev, V. A. and V. I. Petviashvili,: 1994, *Phys. J.* **37**, 699 [Russ. *Izv. Vyssh. Uchebn. Zaved., Fiz.*, No. 7, 118].
Krishan, V., Fernandes, F. C. R., Cecatto, J. R., and Sawant, H. S.: 2003, *Sol. Phys.*, **215**, 147.
Krüger, A.: 1979, *Introduction to Solar Radio Astronomy and Radio Physics,* Reidel, Dordrecht.
Kuijpers, J.: 1975a, *Collective wave-particle interactions in solar type IV radio source*, Ph.D Thesis*,* Utrecht University.
Kuijpers, J.: 1975b, *Solar. Phys.* **44,** 173.
Kubo, M., Yokoyama, T., Katsukava, Y. *et al.*: 2007, PASJ, **59**, S779.
Kuznetsov, A.A.: 2007, *Astron. Lett.* **33**, 319.
Kuznetsov, A.A.: 2008, *Solar Phys.* **253**, 103.
Kuznetsov, A.A., and Tsap, Yu.T.: 2007, *Solar Phys.* **241**, 127.
LaBelle J., Treumann R.A., Yoon P.H., Karlicky M.*:* 2003, *Astrophys. J.* **593**, 1195.
Laptukhov, A. I.: 1991, in *Interplanetary Medium and Magnetospheric Processes*, Nauka, Moscow [in Russian].
Laptuhov, A.I. and Chernov, G.P.: 2006, *Plasma Phys. Rep.* **32**, 866.
Laptuhov, A.I. and Chernov, G.P.: 2009, *Plasma Phys. Rep.* **35**, 160.
Laptuhov, A.I., Chernov, G.P. and Kovalev, V.A.: 2005, in *International Symposium "Astronomy-2005: Current State and Prospects,"* Moscow, 2005, Book of Abstracts, Paper P2.31; Tr. GAISh **78**, 31.
Ledenev, V. G., Karlický, M., Yan, Y., and Fu, Q.: 2001, *Sol. Phys.*, **202**, 71.
Ledenev, V. G., Yan, Y., and Fu, Q.: 2006, *Sol. Phys.*, **233**, 129.
Lin, J., and Forbes, T. G.: 2000, *JGR,* **105**, 2375.
Liu, Y., Luhmann, J. G., Muller-Mellin, R. *et al.*: 2008, *Astrophys. J.* **689**, 563.
Magdalenic´, J., Vršnak, B., Zlobec, P., Hillaris, A., Messerotti, M.: 2006, *Astrophys. J.* **642**, L77.
Mészárosová, H., Karlický, M, Sawant, H. S, Fernandes, F. C. R., Cecatto, J. R., and de Andrade, M. C.: 2008, *Astron. Astrophys*. **491**, 555.
Mollwo, L.: 1983, *Solar Phys.* **83,** 305.
Mollwo, L.: 1988, *Solar Phys.* **116,** 323.
Osten, R.A., and Bastian, T.S.: 2006, *Astrophys. J.* 637, 1016.
Pick, M., De´moulin, P., Krucker, S., Malandraki, O. and Maia, D.: 2005, *Astrophys. J.* **625,** 1019.

Priest, E. and Forbes, T.: 2000, *Magnetic reconnection*, Cambridge Univ. Press.
Roussev, I.I., Forbes, T. G., Gombosi, T.I. *et al.* : 2003, *Astrophys. J*. **588**, L45.
Sawant, H. S., Fernandes, F. C. R., Cecatto, J. R., et al.: 2002, *Adv. Space Res.*, 29, 3, 349
Schwenn, R., Raymond, J. C., Alexander, D. *et al*.: 2006, *Space Sci. Rev.* **123**, 127.
Slottje, C.: 1972*, Sol. Phys.* **25**, 210.
Slottje, C.: 1981, *Atlas of fine Structures of Dynamic Spectra of Solar Type IV-dm and Some Type II Bursts,* Utrecht Observatory.
Stepanov, A.V.: 1974, *Soviet Astron.* **17**, 781.
Stepanov, A.V., and Tsap, Y.T.: 1999, *Astron. Reports* **43**, 838.
Strong, K.T. Bruner, M. Tarbell, T. Title, A.and Wolfson, C.J.: 1994, *Space Sci. Rev.* **70**, 119.
Sych, R.A., Sawant, H.S., Karlický, M., Mészárosová, H.: 2006, *Adv. Space Res.* **38**, 979.
Tan, B. L., Yan, Y. H., Tan, C. M., and Liu, Y. Y.: 2007, *Astrophys. J*. **671**, 964.
Tsuneta, S.: 1996, *Astrophys. J*. **456**, 840.
Tsytovich, V.N.: 1970, *Nonlinear Effects in Plasma,* Plenum Press, New York.
Wang, S.J. Yan, Y.H., Liu, Y.Y., Fu, Q.J. Tan, B.L., Zhang Y.: 2008, *Sol. Phys*. **253**, 133.
Weiland, J. and Wilhelmsson, H.: 1977, *Coherent Non-linear Interaction of Waves in Plasma*, Pergamon Press.
Winglee, R.M. and Dulk G.A.: 1986, *Astrophys. J.* **307,** 808.
Yan, Y., Huang, J., Chen, B., Sakurai, T.: 2007, *PASJ*, **59**, S815.
Zaitsev, V.V., and Stepanov, A.V.: 1975, *Astron. Astrophys*. **45**, 135.
Zheleznyakov, V. V.: 1995, *Radiation in Astrophysical Plasmas*, engl. transl. Kluwer Academic Publisher, Dordrecht (in Russ., Izdat. Nauka, Moscow, 1977).
Zheleznykov, V.V., and Zlotnik, E.Ya.: 1975, *Solar. Phys.* **44**, 461.
Zlobec, P., Karlický, M.: 2008, *Solar Phys.* **246**, 419.
Zlotnik, E.Ya.: 2009, *Cent. Eur. Astrophys. Bull*. **33**, 281.
Zlotnik, E.Ya., Zaitsev, V.V., Aurass, H., Mann, G., Hofmann, A.: 2003, *Astron. Astrophys.* **410,** 1011.
Zlotnik, E.Ya., and Sher, E.M.: 2009, *Izv. VUZov Radiofizika,* **52**, 95 *(Rus), Radiophysics and Quantum Electronics* **52**, 88.
Zlotnik, E.Ya., Zaitsev, V.V., Aurass, H., Mann, G.: 2009, *Solar. Phys.* **255**, 273.